Chapter 3

Surface Structural Chemistry

B. E. Koel[1] *and G. A. Somorjai*[2]

1 Cooperative Institute for Research in Environmental Sciences
and Department of Chemistry, University of Colorado
Boulder, Colorado 80309, USA
2 Materials and Molecular Research Division,
Lawrence Berkeley Laboratory, Department of Chemistry
University of California, Berkeley, California 94720, USA

Contents

1. Introduction: The Atomic and Electronic Structure of Surfaces

The atomic geometry and electronic structure of surface atoms are responsible for the chemical and electronic properties of surfaces. The atomic and electronic structures are rarely separable. However, the experimental techniques used to study these two structural features are different, and therefore they are often separately investigated and discussed. In this review we shall give an overview of what we know about the atomic structure of surfaces and adsorbed monolayers, the methods used to obtain this information, and point

J. R. Anderson et al. (eds.), *Catalysis*

out the importance and relation of surface structure to chemical bonding and heterogeneous catalysis.

Over the past 15 years, there has been a major revolution in the field of surface chemistry that has permitted the atomic scale scrutiny of surface monolayers. The low energy electron diffraction (LEED) technique was developed which enables one to determine the location of ordered layers of surface atoms and of molecules adsorbed on surfaces. High resolution electron energy loss spectroscopy (HREELS) which was also developed over the past ten years can yield vibrational spectra of adsorbed atoms and molecules on surfaces. These two techniques have been used most extensively for studies of the surface structure of single crystal substrates and adsorbed monolayers on these surfaces, and provide information about a large and rapidly increasing number of systems. We have chosen to rely mainly on these two techniques in our studies and the emphasis of this review will primarily be on data from these two methods. However, we will also mention many other promising techniques for surface atomic structure analysis that are available or are being developed. Since detailed investigations of surface structure have mainly used single-crystal substrates under ultrahigh vacuum (UHV) conditions, this review will focus on these systems. We will point out the application of results from these fundamental studies to the understanding of some of the elementary processes in heterogeneous catalysis.

In the next two Sections (2 and 3), we discuss briefly the basic principles and methods of LEED and HREELS for surface structural analysis. Section 4 considers several other methods for studying surface structure. The main part of this review, Section 5, is an assessment of our understanding of the surface structure of clean surfaces, atoms adsorbed on surfaces, and molecules adsorbed on surfaces, as determined primarily by LEED and HREELS. In Section 5.C which considers molecules adsorbed on solid surfaces, we discuss several case studies that illustrate the application of surface structural analysis. The chemisorption of CO is discussed because of its involvement in important catalytic reactions and as a prototype of more complex systems, clearly exhibiting various modes of molecular bonding to surfaces and bond strength variations due to the nature of the substrate. A LEED and HREELS study of benzene chemisorption on Rh(111) illustrates the utility of a combined techniques approach in surface studies. The important area of hydrocarbon reactions is dealt with and elementary chemical transformations are illustrated in alkene adsorption and decomposition on transition metal surfaces. Section 6 contains some future directions in surface structural analysis that we expect to have a major impact on our understanding of surface structural chemistry. Finally, in Section 7, we discuss the structure sensitivity of the surface chemical bond and its implications to catalysis.

In our discussion of surface structure, we will often refer to the periodic geometry of the substrate and of the adsorbed monolayer. The surface unit cell is the basic structural unit in the description of the ordering of surfaces. Often when adsorbates form ordered structures or when reconstruction of the substrate atoms occur, the unit cells of those structures is different from the unit cell of the substrate. When this unit cell is larger than that of the

substrate, the surface lattice is called a superlattice. It is necessary therefore to have a notation that allows the unique characterization of the surface or adsorbate lattice relative to the substrate lattice. Two common notations are used: the matrix notation and the Wood notation [1]. In matrix notation, the unit cell basis vectors ($\mathbf{a}_1$, $\mathbf{a}_2$) of the substrate surface lattice are related to those of the adsorbate ($\mathbf{b}_1$, $\mathbf{b}_2$) by a matrix M:

$$\begin{pmatrix}\mathbf{b}_1\\ \mathbf{b}_2\end{pmatrix} = \begin{pmatrix}M_{11} & M_{12}\\ M_{21} & M_{22}\end{pmatrix}\begin{pmatrix}\mathbf{a}_1\\ \mathbf{a}_2\end{pmatrix} = M\begin{pmatrix}\mathbf{a}_1\\ \mathbf{a}_2\end{pmatrix}$$

The Matrix M uniquely characterizes the relationship between the unit cells. The Wood notation, in which the relationship between the unit cells is somewhat more transparent, can be used when the angles between the pairs of basis vectors are the same for the adsorbate and substrate, *i.e.*, when the angle between $\mathbf{b}_1$ and $\mathbf{b}_2$ is the same as the angle between $\mathbf{a}_1$ and $\mathbf{a}_2$. Then the unit cell relationship is given by, in general,

$$\text{c or p } (v \times w)\ \text{R}\alpha\ .$$

Here v and w are the elongation factors of the basis vectors:

$$v = \frac{|\mathbf{b}_1|}{|\mathbf{a}_1|}, \qquad w = \frac{|\mathbf{b}_2|}{|\mathbf{a}_2|}$$

The angle of rotation between the lattices, i.e., the angle between $\mathbf{a}_1$ and $\mathbf{b}_1$, is α. The suffix Rα is omitted when $\alpha = 0$. The prefixes "c" and "p" mean "centered" and "primitive", respectively, with centered denoting the case where a lattice point is added in the center of the primitive unit cell. The prefix p is optional, and often omitted. The two notations for simple unit cells are easily related. For example, the Wood notation for an overlayer unit cell identical to that of the substrate is p(1 × 1) or (1 × 1), while in matrix notation it is $\begin{pmatrix}1 & 0\\ 0 & 1\end{pmatrix}$. In another slightly more complicated case, the Wood notation is c(2 × 2) = ($\sqrt{2} \times \sqrt{2}$) R45° or in matrix notation $\begin{pmatrix}1 & -1\\ 1 & 1\end{pmatrix}$.

2. The Low Energy Electron Diffraction Technique for Atomic and Molecular Surface Structure Determination

Most of the experiments that are aimed to determine surface structure use a single crystal surface of about 1 centimeter in diameter, placed in an ultra-high vacuum system which is equipped for a variety of surface science techniques. Foremost among them is low energy electron diffraction (LEED) and Auger electron spectroscopy (AES) that determine the atomic structure and composition, respectively, of the surface layers. The surface that is to be studied has to be suitably prepared by ion sputtering and/or chemical treatments to remove surface impurities and then the surface must be

annealed to move atoms into their equilibrium position and to minimize surface structural damage. Figure 1 shows a typical geometry that is utilized in low energy diffraction and other single crystal surface studies.

Electron spectroscopic techniques give information about surfaces due to the high inelastic scattering cross-section of electrons. A "universal curve" for the inelastic mean free path in solids shows that between 10 and 500 eV electron kinetic energy, the mean free path is of the order of 0.4 to 2.0 nm. Figure 2 shows the number of back scattered electrons as a function of their energy when a 2,000 eV electron beam strikes the surface. At 2,000 eV (Region I) there is an elastic peak due to nearly elastically scattered electrons that have lost only small amounts of energy. At higher resolution, this energy region can provide information about atomic vibrations that are in the range of 0 to 0.4 eV. Region II shows inelastically scattered electrons which have caused electronic excitations, along with bulk or surface plasmon excitations. Higher energy losses (Region III) are due to ionizing excitations of electrons and these provide information about the surface composition by identifying the atoms the electrons came from. At very low energies (Region IV), there is a large secondary electron emission background that is due to multiple inelastic scattering that often results in the emission of several electrons of lower energy upon the incidence of one electron of higher energy. In LEED, the elastically backscattered (diffracted) electron fraction (Region I in Figure 2) is used to study the structure of surfaces and adsorbates.

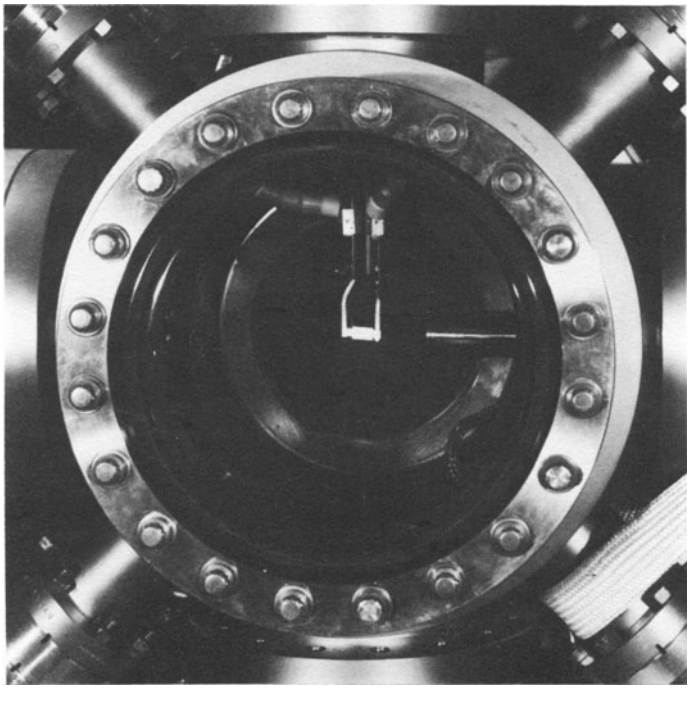

Figure 1. Single-crystal metal sample mounted in an ultra-high vacuum (UHV) chamber prepared for surface studies

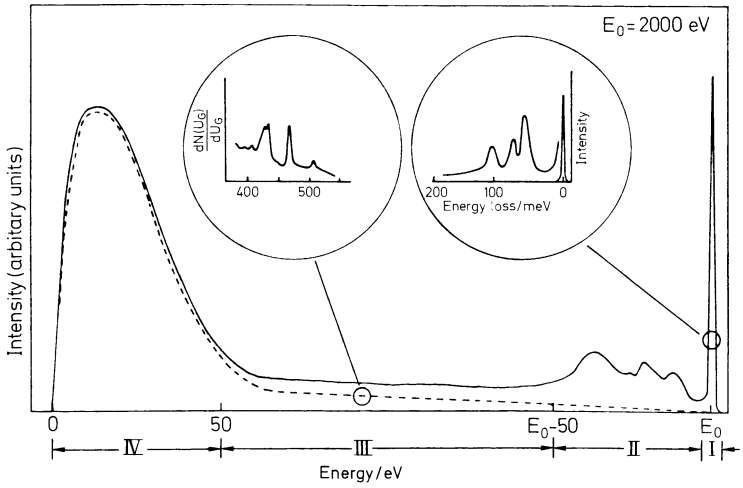

Figure 2. Energy distribution of backscattered electrons. Plot is of the number of scattered electrons, $N(E)$, as a function of their kinetic energy, E

In LEED, a collimated beam of electrons of well-defined (but variable) energy is diffracted by a crystal surface. The electrons are scattered mainly by the individual atom cores of the surface and produce wave interferences that depend strongly on the relative atomic positions of the surface under examination, because of the quantum-mechanical wave nature of electrons.

The de Broglie wavelength of electrons, λ, is given by the formula λ (in nm) $= \sqrt{1 \cdot 5/E}$, where E is measured in eV. In the energy range of 10 to 500 eV, the wavelength varies from 0.39 to 0.055 nm, comparable to interatomic distances. Thus, the elastically scattered electrons can diffract to provide information about the periodic surface structure.

Figure 3 shows the scheme of the LEED experiment. A monoenergetic beam of electrons in the range of 10 to 500 eV is incident on a single crystal. Roughly 1 to 5 percent of the incoming electrons are elastically scattered. A retarding field analyzer separates this fraction, which is then post-accelerated onto a fluorescent screen where the intensity is displayed and may be photographed. If the crystal surface is well-ordered, a diffraction pattern consisting of bright, well-defined spots will be observed on the screen. The sharpness and overall intensity of the spots is related to the degree of order on the surface. When the surface is less ordered, the diffraction beams broaden and become less intense while some diffuse background intensity appears between the beams. The electron beam source commonly used has a coherence width of about 10 nm. This means that sharp diffraction features are obtained only if the regions of well-ordered atoms ("domains") are of the order of $(10\ \text{nm})^2$ or larger. Diffraction from smaller size domains gives rise to beam broadening and finally to the disappearance of recognizable beams from a disordered surface.

The diffraction pattern from the (111) face of a platinum single crystal is shown in Figure 4. The brightness and sharp definition of the diffraction

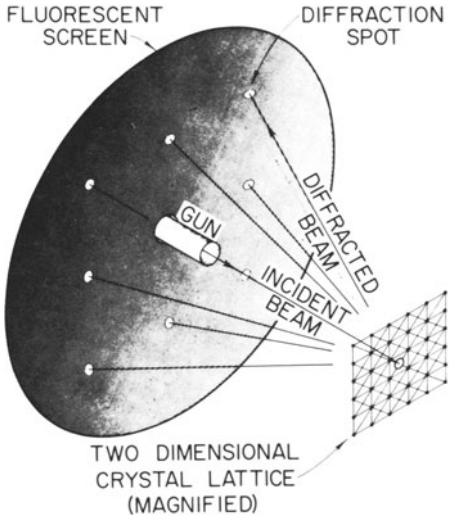

Figure 3. Scheme of the LEED experiment

beams and the weak intensity of the diffuse background clearly indicates a well-ordered surface.

One may distinguish between "two-dimensional" LEED and "three-dimensional" LEED. In two-dimensional LEED one observes only the shape of the diffraction pattern (as seen and easily photographed on a fluorescent screen) [2, 3]. The bright spots appearing in this pattern correspond to the points of the two-dimensional reciprocal lattice belonging to the repetitive crystalline surface structure, *i.e.*, they are a (reciprocal) map of the surface periodicities. Therefore, they give information about the size and orientation of the surface unit cell; this is important information, since the presence of, for example, reconstruction-induced and overlayer-induced superlattices is made immediately visible. This information also includes the presence or absence of regular steps in the surface [4, 5]. The background in the diffraction pattern contains information about the nature of any disorder present on the surface [6]. As in the analogous case of X-ray crystallography, the two-dimensional LEED pattern in itself does not allow one to predict the internal geometry of the unit cell (although good guesses can sometimes be obtained); that requires an analysis of the intensities of diffraction. Nevertheless, two-dimensional LEED already can give a very good idea of essential features of the surface geometry, in addition to those mentioned before. Thus, one may follow the variation of the diffraction pattern as a function of exposure to foreign atoms: it is often possible to obtain semi-quantitative values for the coverage, for the attractive and/or repulsive interactions between adsorbates [7], for some details of island formation [6], etc. The variation of the diffraction pattern with changing surface temperature also provides information about these interactions (in particular at an order/disorder transition) [6], while the variation with electron energy is sensitive to quantities such as surface roughness perpendicular to the surface and step heights [4, 5].

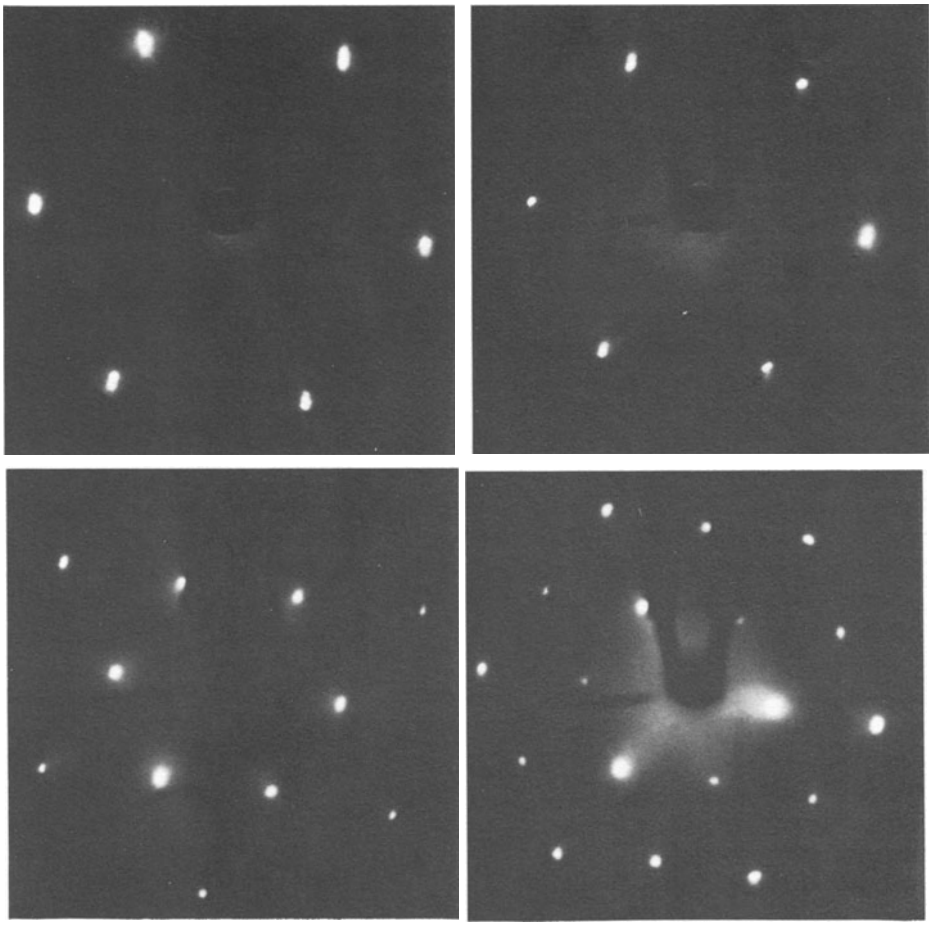

Figure 4. LEED pattern from a Pt(111) crystal surface at 51 eV (upper left), 63.5 eV (upper right), 160 eV (lower left), and 181 eV (lower right) incident electron energy and normal incidence. With increasing energy the diffraction spots converge towards the specular reflection spot, here hidden by the sample

In three-dimensional LEED, the two-dimensional pattern is supplemented by the intensities of the diffraction spots (thereby focusing the attention on the periodic part of the surface structure, *i.e.*, the ordered regions) to investigate the three-dimensional internal structure of the unit cell. This is most readily carried out by considering the variation of the spot intensities as a function of electron energy and/or incidence direction. The pictures in Figure 4 were taken at different incident electron energies. As the electron energies increase, the de Broglie wavelength decreases, bringing in higher order diffraction beams into the view of the fluorescent screen. If the intensity of each diffraction beam is monitored as a function of electron energy, an intensity versus electron voltage curve, or *I–V* curve, is obtained as shown in Figure 5. The fluctuations of the diffraction beam intensities

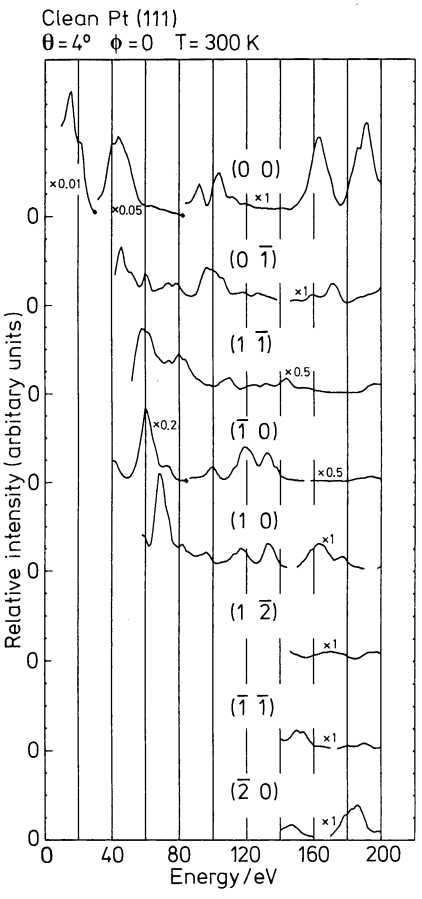

Figure 5. Experimental intensity versus electron energy (I–V) curves for electron diffraction from a Pt(111) surface. Beams are identified by different labels (h, k) representing reciprocal lattice vectors parallel to the surface. Here the angle of incidence was 4° from the surface normal

clearly indicate that diffraction is not two dimensional. The beam as it penetrates the surface undergoes diffraction from the successive layers, providing 3-dimensional diffraction. As a result, the structure of not only the surface layer of atoms but also the positions of atoms in the second and third layers are determined by LEED.

The extreme surface sensitivity of the technique is due to the high elastic as well as inelastic scattering cross sections of the electrons as compared to x-rays. Because of the high scattering cross sections, a large fraction of incident electrons are backscattered in the first two or three layers at the surface. This surface sensitivity, of course, is exceedingly important in surface structural analysis. However, as a consequence, multiple scattering of the electrons cannot be neglected, *i.e.*, there is a significant probability that an electron scattered once will be scattered again before exiting the surface region. Thus, the structure analysis must include multiple scattering of electrons, and in fact, this multiple scattering is very sensitive to the precise locations of atoms and molecules in the surface.

It is necessary to theoretically simulate the electron diffraction in order to extract the atomic positions from the experimental data. This simulation normally must include the multiple scattering of the electrons in the surface region, resulting in so-called "dynamical" calculations [8, 9]. A suitable scattering potential, calculated from first principles, is used for this purpose. A multiple scattering calculation presupposes given atomic positions. Consequently, the simulation must be repeated for a variety of *a priori* plausible surface configurations. For each configuration, the theoretical diffraction intensities are then compared with the experimental data. The best agreement in this comparison occurs for the correct configuration. Refinements of atomic positions can be carried out as desired, usually with the aid of computed reliability factors (R-factors) that remove the subjectivity of visual evaluation which is inevitable when many comparisons must be made.

LEED has developed over the past ten years into a relatively well established technique for surface structure determination and has been the most productive technique used to analyze atomic positions, bond lengths and bond angles at surfaces [2, 8–12]. The largest number of results concern clean, flat (low Miller Index) single-crystal surfaces and atomic adsorbates on them. These have established the technique on a sound and reliable footing and have served as the necessary base for the more recent studies of adsorbed molecules. Overall, over 150 detailed structures have been determined with LEED so far, of which about 10 involve molecules adsorbed at metal surfaces. In addition, hundreds of ordered LEED patterns have been observed and used to understand the two-dimensional periodicity of solid surfaces.

Still, LEED has some limitations. A chemical identification of the surface atoms is not possible by LEED alone. Also, for a LEED structural analysis, it is desirable to first obtain a well-ordered arrangement of the surface. This means studies can be carried out only on single-crystal substrates. Furthermore, atomic and molecular adsorbates preferably should also give an ordered surface structure for LEED analysis. Electron beam damage of molecular adsorbates is currently often a problem, but new developments in the LEED experimental method should reduce this limitation. Also, hydrogen can only be detected in unusual circumstances. Another limitation also concerns the cost of computing which can become large for certain types of structures.

3. High Resolution Electron Energy Loss Spectroscopy (HREELS) as a Probe of Surface Structure

HREELS has undergone an explosive development in the last ten years due to its ability to extract important structural information about atomic and molecular species adsorbed at surfaces [13, 14], and has been applied to a large number (~ 250) of adsorption systems [15]. By a suitable monochromatization of incident electrons of energy 2 to 10 eV and energy analysis of the scattered electrons, small energy losses due to vibrational excitations of surface

atoms and molecules are detectable with an energy resolution of 2.5 to 10 meV (20 to 80 wavenumbers; 1 meV = 8.065 cm^{-1}). This monochromatization and analysis is achieved by using an electrostatic deflection spectrometer, typically using 127° cylindrical or hemispherical sectors.

A spectrometer used in the author's laboratory, which is similar to that used commonly [16], is shown in Figure 6. Thermal electrons from a hot tungsten filament are focussed with an Einsel lens onto the monochromator entrance slit. After exiting the monochromator, the monoenergetic electron beam is focussed on the sample by additional lenses. The sample beam current is 10^{-9}–10^{-11} A. The electrons that are back-reflected from the sample surface are focussed on the analyzer entrance slit and energy analyzed to produce an electron energy loss (vibrational) spectrum. A channeltron electron multiplier with pulse-counting electronics is used to detect the scattered electrons. For specular reflection, typical elastically scattered intensities are 10^4–10^6 counts per second, while inelastic channels have 1–10^4 counts per second. Energy losses of scattered electrons can be measured over a large range, typically 15 to 500 meV (120–4000 cm^{-1}) and higher.

Electrons that are inelastically scattered in the specular direction have undergone a long-range interaction with surface vibrational modes that is similar to the interaction experienced by photons in reflection infrared spectroscopy at surfaces [17, 18]. This interaction is called (dynamic) dipole scattering and involves only those vibrational modes that have a long wavelength in the direction parallel to the surface (these are small-wavevector

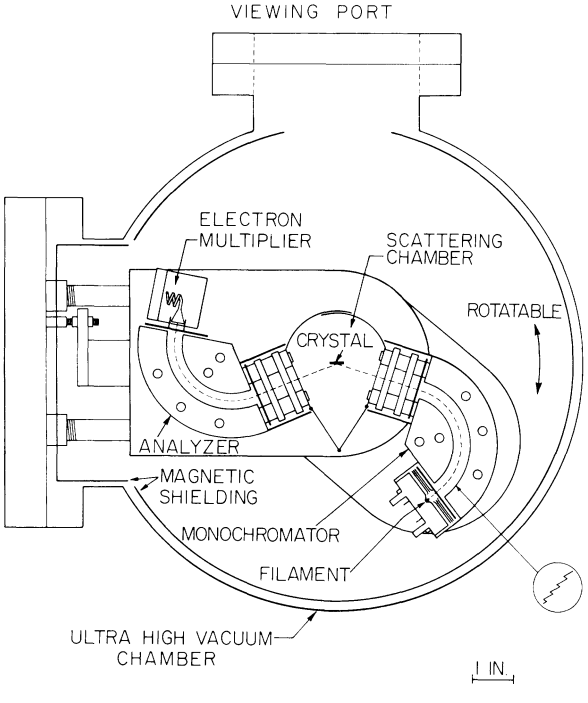

Figure 6. Schematic diagram of the HREELS spectrometer used in our studies. The energy dispersive elements are cylindrical sector analyzers

modes that therefore can only impart momentum to cause a small deviation of the electrons away from specular reflection). The dipole scattering mechanism produces inelastic scattering that is sharply peaked near the specular beam [19–21]. The angle of displacement of this intensity from the specular direction is a function of $\hbar\omega_0/2E$, where ω_0 is the frequency of the vibration and E_1 the impact energy, and for common experimental conditions is 0.1 to 5^0. Note that the large-angle scattering (from the incidence direction to the specular direction) implicit in specular reflection is due mainly to a LEED-like diffraction by the surface (especially the substrate), which usually causes no detectable loss of kinetic energy. A specular HREELS spectrum thus exhibits loss peaks at those energies that correspond to the vibrational frequencies of the molecular (or atomic) species in their adsorbed state on the surface. This allows the ready identification of the adsorbed species by comparison with known frequencies in other circumstances, as in gas-phase molecules and in particular organometallic clusters. Phonons of the substrate can also be detected in this manner [22]; their frequencies generally fall below those of interest in adsorbed molecules.

In dipole scattering from metal substrates, the surface dipole selection rule states that only vibrational modes with a dynamic dipole component perpendicular to the surface can be excited. The physical basis of the selection rule is shown in Figure 7. Any dipole perpendicular to the surface generates an image force in the solid that enhances the strength of the dipole. As a result, it absorbs more energy and can be exited vibrationally quite strongly. Any dipole that is parallel to the surface has an image dipole that tends to cancel it. Therefore, the dipole scattering for dynamic dipoles oriented

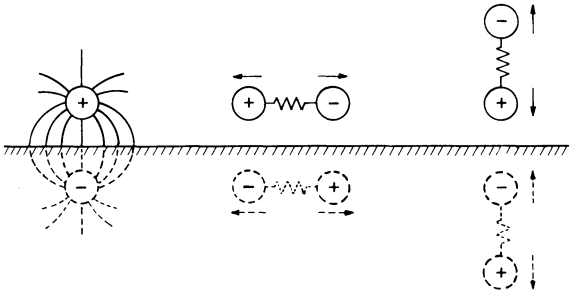

$$\Phi(P_{||}) = P_{||} - \left(\frac{\varepsilon - 1}{\varepsilon + 1}\right) P_{||} = \frac{2}{\varepsilon + 1} P_{||}$$

$$\Phi(P_{\perp}) = P_{\perp} - \left(\frac{\varepsilon - 1}{\varepsilon + 1}\right) P_{\perp} = \frac{2\varepsilon}{\varepsilon + 1} P_{\perp}$$

Figure 7. Physical basis for the dipole selection rule for metal surface. A point charge above the surface induces an opposite charge at the image point below the metal surface, as shown on the left. The same argument holds for the interaction between a dipole and a metal, which is shown in the center and on the right. The relationship of the potential (Φ) for dipole moments parallel ($P_{||}$) and perpendicular ($P_{\perp}$) ro the surface plane is also given in terms of the dielectric constant (ε). In metals, $|\varepsilon|$ is large and thus $\Phi(P_{||})$ is small

parallel to the surface is weak. Of course, we are concerned with the symmetry of the vibrational mode and not the perpendicular or parallel motion of the atoms involved, *i.e.*, there are vibrational modes with a symmetry that generates no dynamic dipole moment perpendicular to the surface even though the atoms move normal to the surface, and vice-versa. The selection rule allows the intensity of energy loss peaks in specular HREELS spectra to be used to determine the symmetry of the adsorbed species and the adsorption site, and to indicate the alignment of an adsorbed molecule with respect to the surface plane. However, this selection rule is sometimes difficult to apply, since the magnitude of the dynamic dipole moment normal to the surface may be small. In these situations, the weak dipole scattering lobe may be obscured by the presence of impact scattering. These difficulties in applying the dipole selection rule can complicate the determination of the symmetry of the surface complex, especially in the case of adsorbed hydrocarbons.

Reflection well away from the specular direction (greater than about 5^0) occurs by so-called impact scattering, which is a short-range interaction with short-wavelength surface vibrations; in the limit it becomes the inelastic scattering of an electron by just one atom of the surface. All vibrational modes

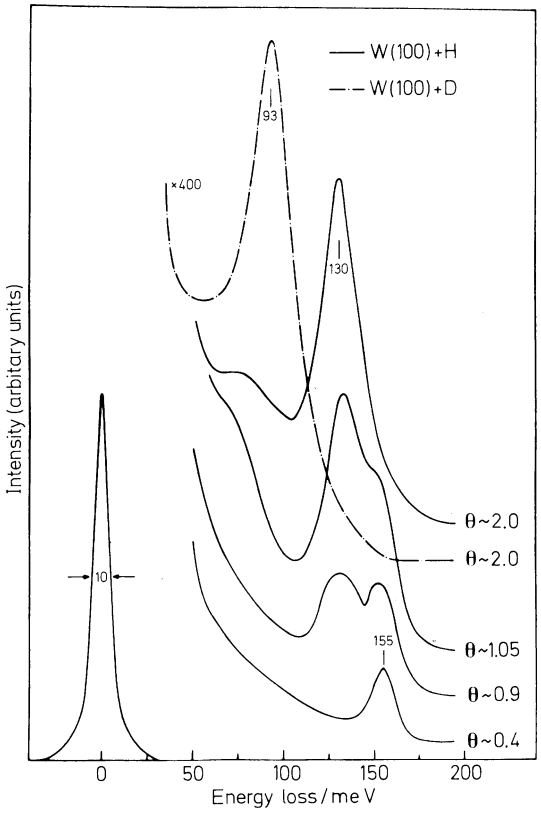

Figure 8. HREELS of H and D atoms adsorbed on W(100) [23]. The elastic peak is shown at left on the plot of scattered electron intensity versus the loss energy (in meV). The H coverage varies from $\theta = 0.4$ to 2.0 (saturation), exhibiting a change in adsorption site, while the D spectrum is shown at $\theta = 2.0$ only. Reproduced with permission from ref. [23]

in principle should be detectable in off-specular HREELS data, except for certain directions not allowed by symmetry. This data is a very useful complement to the specularly measured data. The physical basis of impact scattering is still being investigated, while the transition between impact scattering and dipole scattering is essentially unexplored. New effects may thus still be discovered that can open up unexpected ways of obtaining new information about adsorbed species.

Due to the high electron inelastic cross section, very weak scatterers such as hydrogen can be detected on single-crystal metal surfaces by HREELS. Figure 8 shows the spectrum obtained when hydrogen and deuterium are adsorbed on the W (100) surface [23]. The complexity of the vibration spectra indicates that hydrogen is located in various sites, with various metal hydrogen stretching frequencies on the metal surface. This high sensitivity also makes adsorbed hydrocarbons relatively easier to study than currently possible by other vibrational techniques. For strong scatters, *e.g.* adsorbed CO, HREELS can be used to study concentrations of 0.1 % of a monolayer.

Several other advantages of HREELS can be listed, in addition to the large frequency range and high sensitivity mentioned above. Both disordered and optically rough surfaces can be studied. It does not require long-range ordering of the surface, thereby giving access to the very important low coverage limit of adsorption where adsorbate-adsorbate interactions are negligible. Few techniques can handle as well as HREELS the spectral complications due to several different coadsorbed species. Finally, due to the low incident beam energies and beam currents, HREELS is a non-destructive technique which can be used to probe even the structure of weakly adsorbed molecules or molecules especially susceptible to damage during analysis using other techniques.

There are two main disadvantages of HREELS. First, the assignment of vibrational modes to individual loss peaks may not be unique due to frequency shifts as a result of bonding, especially with the relatively poor instrumental resolution (usually used) as compared to optical spectroscopies. The poor resolution limits somewhat the use of isotopic substitution and makes the analysis of closely spaced vibrational modes difficult to carry out. At present, the resolution (full width at half maximum of the elastically scattered peak) in HREELS is limited practically to $\sim 50\ cm^{-1}$ (see Section 5.C) and studies have often been carried out at resolutions of 80 to 160 cm^{-1}, with peak assignments made more accurately, within 10 cm^{-1}. However, developments in spectrometer design, along with construction of a quiet, ultra-stable HREELS power supply [24], have recently allowed spectra to be obtained from Rh(111) with 20 cm^{-1} resolution. The second major drawback is that the maximum pressure under which spectra can be obtained is about 5×10^{-5} torr due to electron-gas collisions inside the spectrometer. Thus, surfaces during high pressure catalytic reactions and chemisorption at the solid-liquid interface can not be directly studied. Nevertheless, the combination of a high pressure cell inside a vacuum system which has an HREELS spectrometer is helping to bridge this gap [25].

4. Additional Techniques for the Determination of Surface Structure

We will now discuss several other techniques that are useful for surface atomic structure analysis. Several of these have had only minor importance compared to LEED in determining surface structure to date, but their future appears to be bright. Also, the independent verification of surface structures by several techniques leads to increased confidence in the soundness of the results.

The techniques which have been commonly used as structural methods in surface science can be grouped into several classes, as shown in Table 1. Techniques using diffraction and ion scattering are directly sensitive to atomic positions, and have been used widely in studying solid surfaces and adsorbed monolayers. Other techniques that measure vibrational structure, electronic structure, or the angular distribution of desorbed ions are indirectly sensitive to atomic positions by providing information on symmetry, general molecular configuration, and bond angles. These techniques have provided little structural information about clean surfaces, but have been extremely valuable for the study of atomic and molecular adsorbates. Electron microscopic techniques can directly image atomic structure in selected cases, but few surface science-type studies have been made.

The techniques that use electrons as probes must be employed under vacuum conditions, but have the sensitivity to study fractional monolayers of atoms at single crystal surfaces ($\sim 10^{13}$ atoms cm^{-2}). The optical techniques have the large advantage of utility under atmospheric or higher pressures, but usually suffer from sensitivity problems so that well-defined single-crystal surfaces are often not studied. Development of existing and new techniques to bridge these gaps is being aggressively pursued.

LEED is easily the most used diffraction technique for structural analysis, as discussed in Section 2. Two other electron diffraction techniques [26–28] differ from LEED in the range of electron energies used: Reflection high-energy electron diffraction (RHEED) uses 1–10 keV electrons and Medium-energy electron diffraction (MEED) bridges the gap between LEED and RHEED. Multiple scattering of the electrons occurs at these energies, as in LEED. MEED takes advantage of the larger amount of information in the I–V curves at energies up to 1000 eV, but Debye-Waller effects can require cold temperatures for the experiments. RHEED can be used to probe to a depth of 2–10 nm and give information on structure in the near surface region.

Several techniques have been developed that are based on Angle-resolved photoelectron spectroscopy (ARPES). These methods take advantage of the diffraction of the outgoing photoelectron when atoms in the solid surface are photoionized. The physics of these methods is similar to LEED, but in these cases the electron source is internal to the sample. Angle-resolved ultraviolet photoelectron spectroscopy (ARUPS) and Angle-resolved X-ray photoelectron spectroscopy (ARXPS) have been used successfully [29, 30]

Table 1. List of major techniques that are used to study surface structural chemistry

Diffraction Techniques
LEED — Low-energy electron diffraction
MEED — Medium-energy electron diffraction
RHEED — Reflection high-energy electron diffraction
ARPES — Angle-resolved photoelectron spectroscopy
Atom diffraction
Neutron elastic diffraction
Ion Scattering Techniques
HEIS — High energy ion scattering
MEIS — Medium energy ion scattering
LEIS — Low energy ion scattering
Vibrational Spectroscopies
HREELS — High resolution electron energy loss spectroscopy
ITAS — Infrared transmission-absorption spectroscopy
IRAS — Infrared reflection-absorption spectroscopy
Raman scattering
SERS — Surface enhanced Raman scattering
IETS — Inelastic electron tunneling spectroscopy
NIS — Neutron inelastic scattering
PAS — Photoacoustic spectroscopy
Ion Desorption Techniques
ESD — Electron stimulated desorption
ESDIAD — Electron stimulated desorption ion angular distribution
PSD — Photon stimulated desorption
SIMS — Secondary ion mass spectroscopy
Electronic Structure Spectroscopies
UPS — Ultraviolet photoelectron spectroscopy
XPS — X-ray photoelectron spectroscopy
AES — Auger electron spectroscopy
INS — Ion neutralization spectroscopy
SPIES — Surface Penning ionization electron spectroscopy
Techniques Sensitive to Absorption Coefficient Modulation
SEXAFS — Surface extended x-ray absorption fine structure
XANES — X-ray absorption near-edge structure
EAPFS — Extended appearance potential fine structure
Electron-Optical Techniques
SEM — Scanning electron microscopy
TEM — Transmission electron microscopy
STEM — Scanning-transmission electron microscopy
Other Techniques
TDS — Thermal desorption spectroscopy
Work function measurements

to determine atomic and molecular symmetries, and also geometries at surfaces when combined with dynamical calculations, but their utility has been limited somewhat by larger computational efforts than in LEED (at least at lower energies) and uncertainty in final state relaxation energies. Polarization-dependent ARUPS (PARUPS) has also been used. Normal photoelectron diffraction (NPD) and Angle-resolved photoelectron diffraction fine structure (ARPEFS) methods [31, 32] are potentially as powerful as LEED, but only a few studies of this kind have been made.

Atomic and molecular beams also readily diffract from surfaces [33, 34]. For example, He atoms with thermal energies of 20 meV have a de Broglie wavelength of 0.1 nm. Helium is the particle most commonly used due to its low mass and its chemical inertness, but Ne, H_2, HD, H, and D have also been used. These techniques have extremely high surface sensitivity and are non-destructive. In addition to the atomic positions, atom scattering gives additional information on the electronic charge distribution at surfaces.

The angular distribution and intensity of ions scattered from a surface in channeling and blocking experiments give information on surface structure [35]. Several ion scattering spectroscopies differ only in the incident kinetic energies of the ions used: High-energy (HEIS) [36] with 0.4 to 2 MeV ions, Medium-energy (MEIS) [35] with 0.1 to 0.4 MeV ions, and Low-energy ion scattering (LEIS) [37] with ions of less than 400 keV energy. Depending on the energy and incidence direction the depth resolution can vary from one monolayer to 30 nm. At higher energies a binary collision model for the ion scattering is adequate (Rutherford backscattering) and a quantitative evaluation of the chemical composition of the surface can be made. At lower energies where the depth resolution is better, the main sources of error in the structural analysis are due to uncertainty in the ion-atom scattering potential and multiple scattering effects.

There are many methods sensitive to the vibrations of surface atoms [38–41]. All of these methods indirectly give information on the atomic structure of surfaces through adsorption site symmetries, bond orders and general molecular configurations, as does HREELS (Section 3). Figure 9 compares the vibrational spectra obtained for CO adsorbed on dispersed rhodium particles on alumina by three techniques: (a) HREELS [42], (b) Infrared transmission-absorption spectroscopy (ITAS) [43] and (c) Inelastic electron tunneling spectroscopy (IETS) [44]. It is clear that all of these vibrational techniques provide complementary information about the structure of adsorbed molecules.

Techniques that take advantage of the absorption of infrared radiation by characteristic vibrations at surfaces include Infrared reflection-absorption spectroscopy (IRAS), and Infrared transmission-absorption spectroscopy (ITAS) [41]. Each of these techniques have somewhat different advantages and disadvantages, but several broad generalizations can be made. Work on single-crystal surfaces is difficult except for studies of vibrational modes with large dynamic dipole moments, *e.g.*, the C—O stretching mode in adsorbed CO, and only a couple of studies of hydrocarbons adsorbed on single crystal metal surfaces have been made. The accessible range of vibrational energies

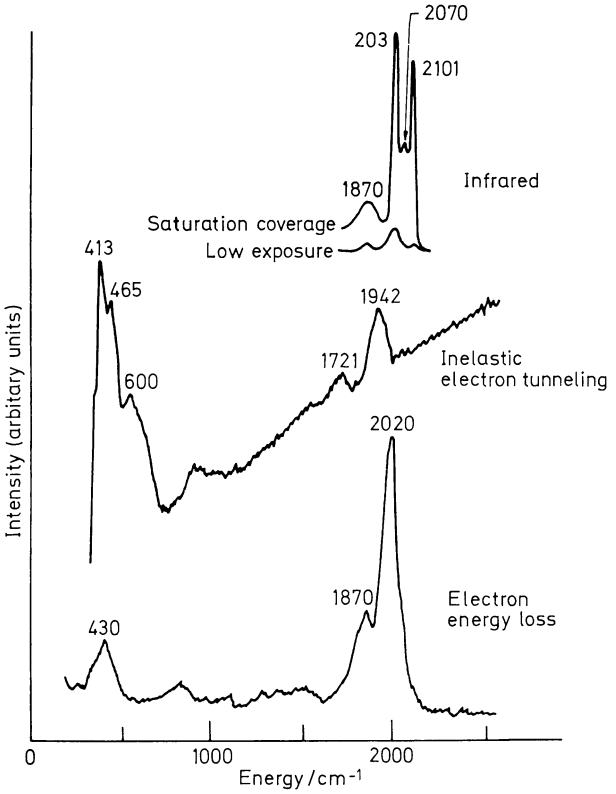

Figure 9. Vibrational spectra taken by three different techniques for CO adsorbed on Rh supported on alumina. In the infrared spectra [43], the high resolution possible with optical techniques is evident. The inelastic electron tunneling spectrum [44] shows the downshift in the C—O stretching vibrations characteristic of this technique and relatively strong low frequency modes. The HREELS spectrum [42] shows the C—O stretching frequencies as a broad envelope of those observed in the infrared spectrum

is usually limited so that the interesting region of metal-atom stretching and bending modes usually cannot be studied. The resolution attainable is very high (0.1 cm^{-1}) so that instrumental broadening of the vibrational lines can be made negligible. This allows studies of the lineshapes, and also the detection of adsorbed species with only slightly different adsorption geometries. Importantly, the use of photons enables one to carry out studies on surfaces under high gas pressures or in the presence of liquids. In a new related development, the first observation of thermally emitted infrared radiation from both metal-carbon and C—O vibrational modes of CO adsorbed on Ni (100) has been made [45].

Surface enhanced Raman scattering (SERS) [46] has been very usefully applied, especially to studying vibrations of molecules adsorbed at surfaces of electrodes in solution. Limitations on the nature of the substrate that can be used (mainly "roughened" Ag, Cu, Au) and the uncertainty on the details of the scattering mechanism have prevented broad applicability of SERS as

a structural probe. Through careful and sensitive detection schemes, non-enhanced Raman scattering has been observed from pyridine on a Ag(111) single-crystal surface [47], and similar studies should be widely applicable to other systems. Also, Raman scattering from near-surface layers (~ 20 nm) can be used to observe phonon modes of oxides and compounds, which often fingerprint the identity of these layers.

Other vibrational techniques include Neutron inelastic scattering (NIS) [48], Inelastic electron tunneling spectroscopy (IETS) [49], and Photoacoustic spectroscopy (PAS) [50]. None of these techniques require vacuum, but they can only be employed for studies of relatively high surface area materials. NIS can only observe vibrations of H or D atoms, but can examine optically opaque samples. The scattering intensities give useful information since the atomic scattering cross-sections are known. IETS has been used to study many large organic molecules adsorbed at surfaces, but suffers mainly from problems associated with the possible influence of the metal counter-electrode.

Ion desorption induced by bombardment of the surface by electrons (Electron stimulated desorption, ESD) [51], photons (Photon stimulated desorption, PSD) [52], or ions (Secondary ion mass spectroscopy, SIMS) [53] can also be monitored to give structural information. The ion desorption thresholds (for the ion yield versus incident excitation energy) in ESD and PSD can often be related to electronic levels of surface atoms and used to determine the nature of the local atomic environment of the bonding site, *i.e.*, the identity of the atoms to which the species was originally bound. Especially useful is the ESD ion angular distribution (ESDIAD) technique for determining molecular structure at surfaces [54]. In this technique, desorbed ions produce spots on a fluorescent screen, and the spot distribution can be used to directly determine bond angles in molecular species.

There are several methods that measure the electronic structure of atoms and molecules at surfaces, and thus are indirectly sensitive to atomic structure. Ultraviolet (UPS) and X-ray photoelectron spectroscopy (XPS) have been used extensively in surface analysis and can give qualitative information about surface structure [55, 56]. The valence electronic density of states can be measured and energy level shifts can be used to determine the atoms involved in chemisorption bonds. In addition, chemical shifts in core level binding energies measured in XPS can often be used to distinguish between atoms in the adsorbed state, atoms incorporated within the first layer, and atoms which have penetrated several layers to form compounds. Chemical shifts and line-shape changes in Auger electron spectroscopy (AES) have been shown to also give valuable structural information [57, 58]. Two electronic spectroscopies give information on the density-of-states distribution from the outer part of the solid-vacuum interface: Ion neutralization spectroscopy (INS) [59] and Surface Penning ionization electron spectroscopy (SPIES) [60, 61] or Metastable deexcitation spectroscopy (MDS) [62].

By using synchrotron radiation and monitoring the total electron yield, Auger electron yield or ion yield, one can measure modulations in the photo-absorption cross-section for surface atoms [63, 64], analogous to EXAFS

[65]. Surface extended X-ray absorption fine structure (SEXAFS) is a technique based on this observation and is a powerful source of information about the local environment of selected atoms on surfaces with or without long-range order. Use of this technique has allowed the determination of adsorption sites and bond lengths of fractional monolayers of atoms. Another technique, X-ray absorption near edge structure (XANES), also called Near-edge X-ray absorption fine structure (NEXAFS) [66], uses the yield structure within the first 50 eV of the absorption edge. The fingerprint of this region has been shown to be sensitive to the unoccupied electronic density-of-states and coordination symmetry of surface species. Extended appearance potential fine structure (EAPFS) [67], also analogous to EXAFS, probes the short-range order of a particular element. EAPFS does not require synchrotron radiation (only an electron gun and LEED retarding analyzer) and can be used to study surface atoms in monolayer concentrations.

Using electron optical techniques, Transmission (TEM), Scanning (SEM) and Scanning transmission electron microscopy (STEM) can be used for direct imaging of the structure of solid surfaces [68–70]. TEM and STEM have allowed resolution of individual atoms. These techniques are usually limited by electron-atom cross sections to heavy atoms on light substrates and to operation in relatively poor vacuums ($> 10^{-6}$ Pa) with high magnetic fields. Adsorbed molecules cannot be studied due to electron beam damage. Also, in transmission modes it is difficult to separate the effects of *two* surfaces. However, the potential for electron microscopy to study the atomic structure of surfaces is great.

Two other techniques give indirect information about the atomic geometry of adsorbed monolayers on solid surfaces. Thermal desorption spectroscopy (TDS) [71] can be used to detect different bonding states of adsorbates by measuring the heat of desorption from these states. The relative populations of the bonding states, and sometimes the absolute coverage, can be found by integrating the spectra. Work function measurements [72] detect changes in charge distribution at the surface. Even though the work function change does not relate simply to the adsorption geometry, measurements can often indicate the general bonding configuration and direction of charge transfer between adsorbate and substrate atoms.

5. Structure of Solid Sufaces

A. The Atomic Structure of Clean Surfaces

The structure and bonding of an adsorbed species is greatly influenced by the structure of the substrate. In order to explore the structural sensitivity of chemical bonding and to obtain structural information on adsorbates, we must know the atomic structure of clean surfaces prior to adsorption. It is also important to know whether the presence of the adsorbate substantially alters the geometric structure of the substrate. Over the past ten

years a good picture has emerged of the details of atomic structure of many surfaces of metals and semiconductors.

Two major phenomena are found: bond length relaxation and reconstruction. Relaxation causes a contraction in the distance between the first and the second layers of atoms at the surface; such relaxations sometimes extend to deeper layers. The interlayer distance between the 1st and 2nd layers may contract up to 15% with respect to interlayer distances in the bulk material. The more open the surface, that is the lower the surface density of atoms, the larger is the relaxation. The precise location of atoms in the first layer does not noticeably change parallel to the surface, only their location in the direction perpendicular to the surface shows alterations. This phenomenon can be understood if we assume that the surface is an intermediate between the diatomic gas phase molecule of the same atomic number and atoms in the bulk. The diatomic molecules have much smaller atomic distances than bulk atoms that have very large coordination numbers, namely 8 to 12 nearest neighbors. In the surface, because of the anisotropy of location and the reduced number of nearest neighbors, there is a contraction of the top interlayer distance.

Reconstruction of the surface occurs when the forces on the surface atoms in the solid are very large and the atoms are forced to move to new atomic locations in order to minimize their surface energy. In this case, the atoms seek new locations in both perpendicular and parallel directions to the surface, which results in new surface structures. LEED diffraction patterns are observed that are very different from what is expected from the projection of the bulk unit cell to the studied surface. The diffraction pattern from a Pt (100) surface is shown in the upper left panel in Figure 10. The LEED pattern and structure that one would expect from the projection of the bulk unit cell is shown on the right and is a square unit mesh. The approximate structure of the clean reconstructed surface is shown in the lower left panel. While the LEED pattern was published in 1965, a solution of the surface structure was reported only in 1981 [73]. The surface platinum atoms are reconstructed into an hexagonal configuration; the coincidence of atomic positions in this reconstructed hexagonal top layer and the unreconstructed second layer gives rise to the complicated diffraction pattern that is shown in Figure 10. The variation in the number of nearest neighbors forces the surface atoms into an undulating configuration. Since buckling increases the total energy, the atoms move into positions that minimize the surface undulation. The precise location of atoms in this reconstructed surface is governed by a delicate balance of forces. Upon adsorption of even small amounts (several percent of a monolayer) of a chemisorbed species such as carbon monoxide or hydrocarbon molecules, the atoms in this reconstructed surface snap back to the equilibrium position that they would have in the bulk: a square unit mesh appears, as shown in the upper right panel of Figure 10. On desorption of these molecules, the clean surface shows the reconstructed surface structure again.

It appears that the (100) crystal faces of gold, platinum, and iridium all show the formation of large superlattices, e.g. (5×1) or (5×20) reconstruc-

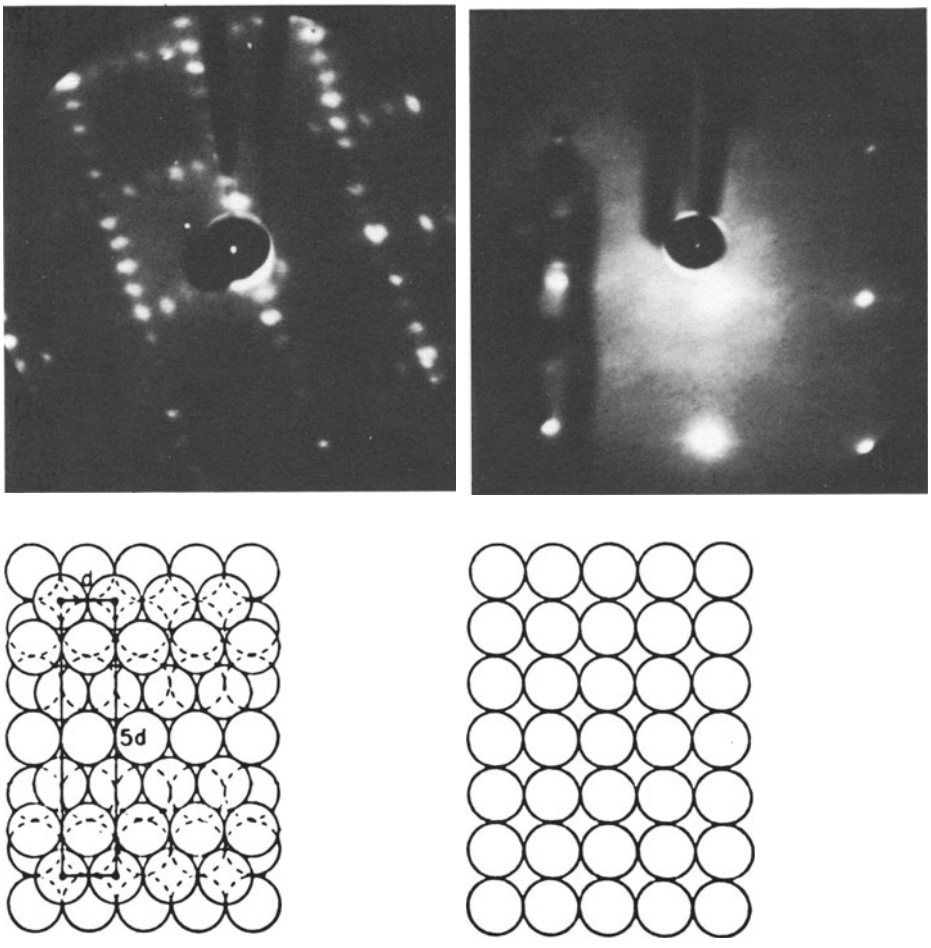

Figure 10. Left: Diffraction pattern and model of the surface structure for the (5×1) surface reconstruction of the Pt(100) crystal face. Right: Diffraction pattern and surface structure that might be expected for the Pt(100) surface assuming simple termination of the bulk lattice

tions [73]. The (110) faces of Au, Pt, and Ir often exhibit $(n \times 1)$ (with $n = 2, 3, 4$) reconstructions [74]. The "missing row" model best explains several of these systems. In this model, small facets of the (111) face are built. The driving force is the lower free energy of the (111) face. The tungsten and molybdenum (100) crystal surfaces also exhibit reconstruction that have been reviewed recently [74a].

Reconstructions are generally observed on semiconductor surfaces, often with several different metastable reconstructions observed for the same compound. A model of the surface structure of the reconstructed Si (100) surface [75] is shown in Figure 11. In this case, one may consider the silicon surface atoms as existing in dimers with troughs in between. The contraction actually permeates at least three layers and so the effect of sur-

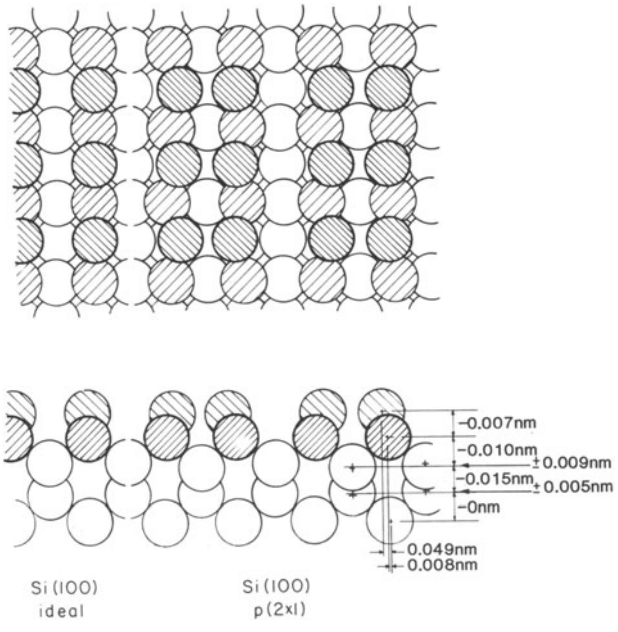

Figure 11. Top and side views of ideal bulk-like Si(100) at the left, and the Si(100) p(2 × 1) reconstruction. Layer-spacing contractions and intralayer atomic displacements relative to the bulk structure are given. Shading differentiates surface layers

face reconstruction is deeper than just the top surface layer. The reconstructions in semiconductors are throught to be due to rehybridization of the orbitals of the surface atoms. Several recent articles cover this exciting area of semiconductor surface structure [76–79]. The advent of increased computing power is currently revolutionizing our ability to understand the microscopic details of complicated reconstructions.

1. Atomic Structure of Unreconstructed Low Miller Index Planes of Transition Metal Surfaces

One can generally observe very small contractions (1–4%) of the bond lengths between the surface atoms and the second-layer atoms for the relatively open faces, such as bcc (100), fcc (110), bcc (111), and fcc (311). This does not result in a reconstruction of the surface layer. The effect of adsorbates on such relaxed surfaces is to restore the bond lengths to their bulk values, or sometimes even to lengthen them.

Contraction or relaxation of atoms at open crystal surfaces is due to the reduction of the positive surface free energy if the surface becomes less rough on the atomic scale. Also, with fewer neighbors the two-body repulsion energy is smaller, allowing greater atomic overlap at shorter bond lengths.

2. The Atomic Structure of High Miller Index Stepped and Kinked Surfaces

When crystals are cut along high Miller index directions, the surfaces often assume sterned ordered, configurations.

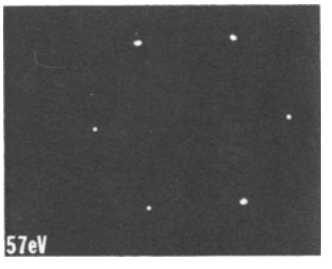

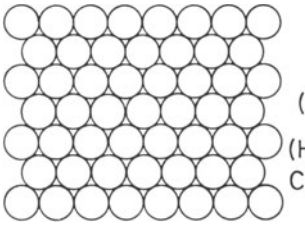

Pt (111)

a

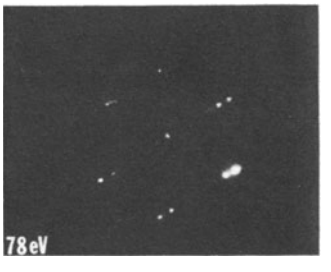

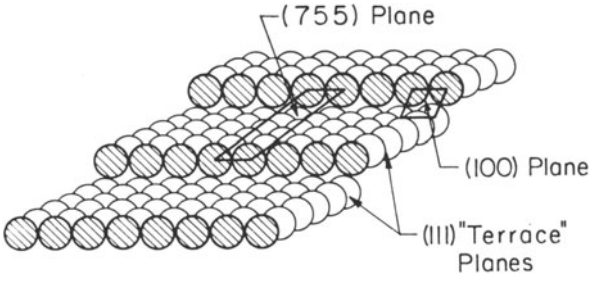

Pt (S)-[6 (111)x(100)]↔Pt (755)

b

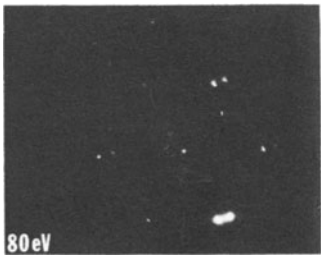

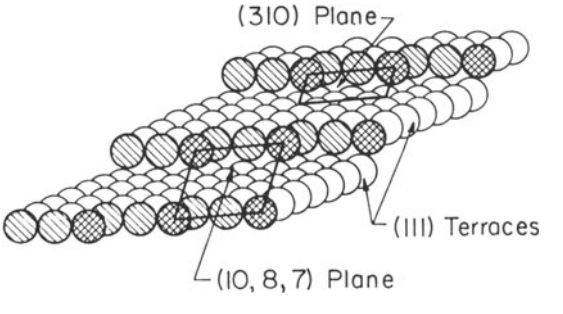

Pt (S)-[7 (111)x(310)]↔Pt (10,8,7)

Figure 12. LEED patterns (left) and surface structures (right) of **a** flat, **b** stepped, and **c** kinked platinum surfaces

These periodic steps in the surface produce recognizable diffraction features, permitting the determination of the height and orientation of the step as well as the terrace width. The orientation of the steps and terraces that are stable correspond normally to those of the highest density atomic planes: (111), (100) and (110) for the fcc and the bcc crystals. By changing the angle of the cut, the terrace width and the step density can be altered. By cutting crystals in such a way that even the steps have high Miller indices, one obtains kinked surfaces. Figure 12 shows structures and diffraction patterns obtained for clean platinum surfaces with (111) terraces and high densities of steps and kinks. The splitting of the diffraction beams is characteristic of the new periodicities introduced by the periodic arrangements of atomic steps on the surface.

Atoms at kink sites have even lower numbers of nearest neighbors than atoms in stepped positions. The heats of adsorption of atoms and molecules at these different sites are likely to be different. As a result, their chemical activities in various rearrangement or dissociation reactions at these sites are different. It is therefore very important to study the effect of changing atomic structure on the location, bonding, and of atoms and molecules on solid surfaces.

The ordered, one-atom height step and periodic terrace configuration appears to be the stable surface structure for many high Miller-index surfaces of metals. Upon heating to near the melting point the steps disorder but reorder again when annealed at lower temperatures. In the presence of a monolayer of oxygen, carbon, or sulfur, many stepped surfaces undergo restructuring. The step height and terrace width may double or faceting may take place whereby the step orientation becomes more prominent than the terrace orientation, giving rise to new diffraction features that are detectable by LEED. The driving force for this surface restructuring in the presence of adsorbates appears to be the difference in chemical bonding of adsorbates to the different crystal faces of the metal which alters the relative surface free energies of the crystal faces. Surfaces that have the lowest free energies when clean become less stable than other crystal faces when covered with adsorbates.

B. The Structure of Adsorbed Atoms on Solid Surfaces

1. Non-Metal Adsorption

The various high symmetry adsorption sites on solid surfaces with low Miller indices are shown in Figure 13. Most atoms whose adsorption and surface structure have been studied by LEED prefer these sites with highest symmetry. It appears that the atoms generally occupy positions with the largest number of metal nearest neighbors and this allows the greatest binding energy between adsorbate and substrate atoms. Figure 14 shows the interatomic distances that were obtained from the surface structures along with the range of

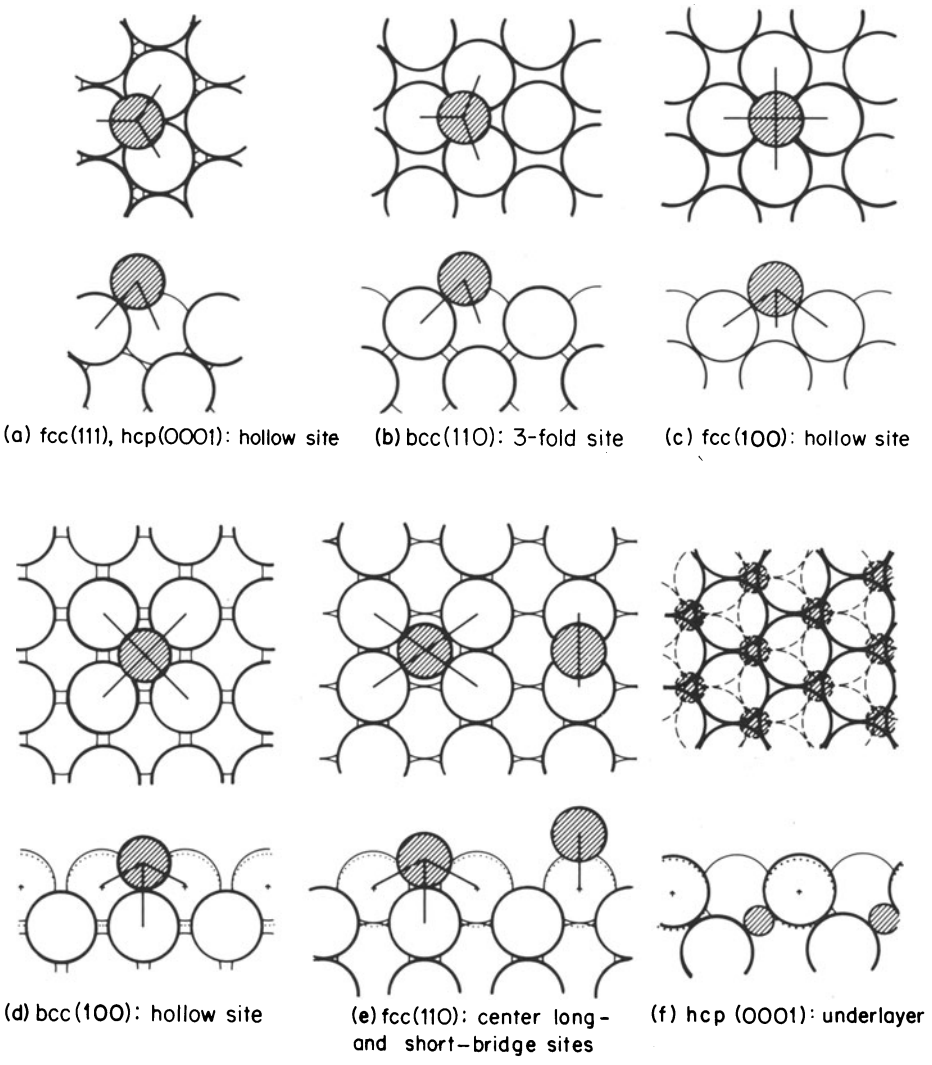

Figure 13. Top and side views (in top and bottom sketches of each panel) of adosprtion geometries on various metal surfaces. Adsorbates are drawn shaded. Dotted lines represent clean surface atomic positions.

interatomic distances that are indicated from X-ray or electron diffraction studies of bulk compounds or gas phase molecules. It appears that the bonding as judged by the interatomic distance for surface atoms falls in the range of bonding found for compounds in the solid state or in the gas phase. This in most cases indicates covalent bonding. Thus, the surface bonding is not qualitatively different from that found in other phases. In the right side of

Figure 14, the ionic character of the bond is shown, as judged by the work function change that accompanies adsorption. The ionic character is very small indeed. It appears that this is an additional confirmation of the covalent bond character of these surface phases.

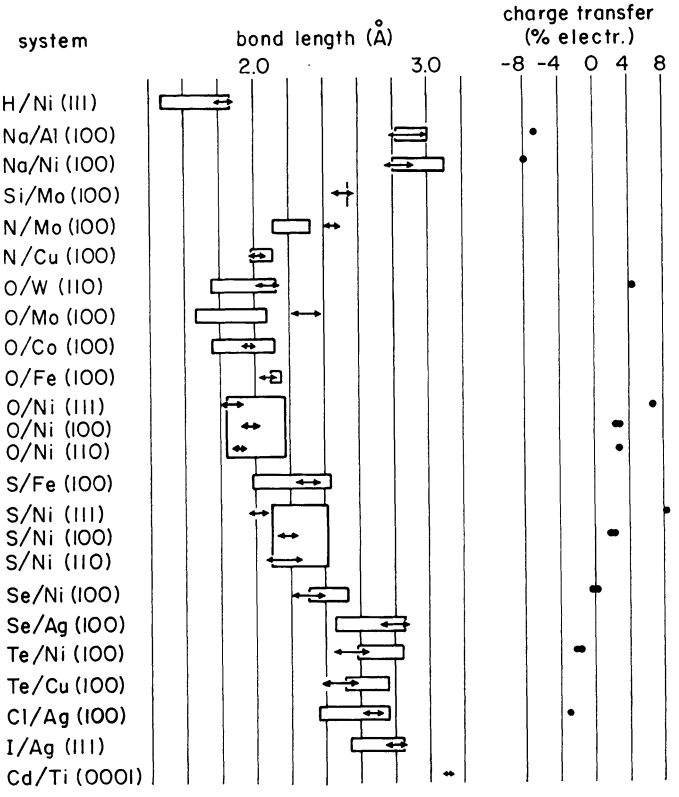

Figure 14. (Left) Comparison of adsorption bond lengths at surfaces (arrows show uncertainty) with equivalent bond lengths in molecules and bulk compounds (blocks extending over range of value found in standard tables). (Right) Induced charge transfer for adsorption

In some cases adsorption results in surface reconstruction. For example, when oxygen adsorbs on the Fe(100) surface [80] or sulfur adsorbs on the Fe (110) surface [81], the surface layer consists of both adatom and iron atoms in the same plane as a precursor to the formation of iron compounds. Reconstruction occurs when the adsorbate-substrate bond is stronger than the bonds between substrate atoms. It is likely that oxidation or other compound formation is accompanied by surface reconstruction. Future studies will certainly explore the role of reconstruction on the initial state of bulk compound formation. Under some conditions a small atom assumes

a position under the surface. The systems N/Ti(0001) [82], O/Al(111) [83], and H/Pd(110) [84] illustrate this point.

2. *Adsorption and Growth of Layers of Metals on Surfaces of Other Metals*

At low coverages, the adsorbate-substrate interaction is dominant and when one metal is deposited on another metal, it is usually found by LEED studies that the surface structure of the deposited metal follows the periodicity of the substrate metal. For example, when gold is deposited on the Pt(100) surface, the gold atoms locate with the periodicity provided by the platinum atoms [85]. This forces the gold atoms into a different interatomic distance than in its own lattice. That in turn may change not only its geometric structure, but also its electronic properties. For this and many other systems, the forces that control epitaxy, the strong interaction between adsorbate and substrate, seem to predominate and control the atomic surface structure.

The relative importance of adsorbate-adsorbate interactions increases at higher coverages and can be dominant especially for large radius metallic adatoms (*e.g.*, K, Rb, and Cs). Thus, at higher coverages, the adsorbate may continue to follow the substrate periodicity, or form coincidence structures, or new periodicities that are unrelated to the substrate periodicity. For example, alkali adatoms tend to form incomensurate hcp layers on any metal substrate.

Still, when gold is condensed in multilayers over platinum surfaces, the gold interatomic distance remains controlled by platinum for the first ten layers of gold [85]. Thus, the effect of the substrate that controls the structure of the adsorbed metal is felt during the growth of the thin metal film. The dominance of epitaxy in metal-metal interactions provides an opportunity to deposit metal monolayers and thin films with interesting atomic and electronic structures. This is an area of fruitful research for the near future.

C. Surface Structure of Molecules on Solid Surfaces

A large number and wide variety of ordered monolayers of adsorbed molecules have been observed by LEED and studied by many other techniques [86]. Still, very few adsorbed molecular structures have been analyzed by LEED surface crystallography or other techniques to yield accurate atomic positions and bond lengths.

Associatively adsorbed CO is the only diatomic molecule studied in this manner to date, and the adsorption geometry of CO on several metal surfaces has been determined by LEED crystallography. These are shown in Table 2, in which we list the results for those CO adsorption systems that have been analyzed by both HREELS and LEED. In these cases, the CO molecules are found to stand perpendicularly to the surface in either top sites or bridge sites (hollow sites on clean metal surfaces are rarely occupied by CO). In addition, almost all of the above systems have been studied by other

Table 2. Metal carbonyl structures and CO stretching frequencies for surfaces and for clusters. The frequencies (measured by HREELS or IR) are classified qualitatively according to the customary adsorption site assignment, for comparison with the site determined by LEED. For clusters the stars indicate the range in which CO stretching frequencies fall. The CO bond length (d_{CO}) and metal-C bond length (d_{MC}) are indicated, together with the corresponding metal-C layer spacing ($d_{\perp MC}$) and an effective carbon radius (r_c) obtained by subtracting the bulk or cluster metallic radius from the metal-C bond length.

	CO Stretching Frequency (cm^{-1})			Site from LEED	d_{CO}/nm	$d_{\perp MC}$/nm	d_{MC}/nm	r_c nm
	hollow 1850	bridge 2000	top					
Surfaces								
Ni(100) + c(2×2) CO			2069	top	0.115	0.176	0.176	0.052
Co(100) + c(2×2) CO			2079–2089	top	0.113	0.190	0.190	0.062
Pd(100) + (2$\sqrt{2}$×$\sqrt{2}$) R45° 2 CO		1903–1949		bridge	0.115	0.136	0.193	0.056
Rh(111) + ($\sqrt{3}$×$\sqrt{3}$) R 30° CO			2020	top	0.107	0.195	0.195	0.061
Rh(111) + (2×2) 3 CO		1870	2070	top + bridge	0.115	0.187	0.194	0.060
					0.115	0.152	0.203	0.069
Free CO			2143		0.115			
Organometallic Clusters								
Ni-metal top			*		0.101–0.116		0.175 0.189	0.056 0.072
bridge		*			0.107–0.117		0.182–0.191	0.065–0.074
Rh-metal top			*		0.109–0.117		0.182–0.191	0.043–0.050
bridge		*			0.114–0.117		0.200 0.209	0.058–0.059
hollow	*				0.115–0.120		0.217–0.223	0.078 0.082

techniques, including those that reveal the electronic structure at the surface, so that a very good picture of how CO bonds to metal surfaces is emerging [87].

It is interesting to compare the surface structure of CO as determined by several techniques. Duke [76] has reviewed the history of structural studies for one particular case, that of Ni(100) + c(2 × 2) CO. This is particularly informative since it compares the results from the first LEED intensity measurements in 1965 with all of the later studies by LEED and other techniques (UPS, ARUPS, HREELS, ARXPS) up to 1981. Agreement on the structure of this system by many different techniques provides confidence in the determination of adsorption site symmetries and bond lengths by the application of these techniques.

LEED intensity analyses have been carried out for acetylene adsorbed on several metal surfaces: Pt(111) [88], Ni(100) [89], and Ni(111) [90]. The LEED crystallography results on the ordered (2 × 1) structures of acetylene show that adsorbed acetylene is strongly distorted (to $\sim sp^3$ hybridization) and forms di-σ bonds to the surface. These results are supported by a reinvestigation of published UPS and HREELS data [91].

Fragmentation of alkenes can give ordered hydrocarbon species which can also be studied by LEED crystallography, and these systems will be discussed in Section 5.C.3.

Vibrational spectroscopy (mainly HREELS), ESDIAD, and ARUPS have been especially useful for determination of the general molecular structure of molecules at metal single crystal surfaces. HREELS has been used to study CO adsorption on about 25 single crystal substrates, and for these systems it readily distinguishes between bridge-bonded or atop adsorption sites. Molecularly adsorbed acetylene, ethylene, benzene, and a handful of other small organic molecules have been studied by HREELS on a number of metal surfaces [15]. These studies indicate associative or dissociative adsorption, molecular distortion and bonding mode, and the symmetry of the surface complex (the adsorbed molecule plus adsorption site). ESDIAD has been used to study about 20 adsorbed molecules, mostly di- and triatomic ones [54]. The structural assignment from these studies mainly determines which end of the molecule is bound to the surface, whether the molecular is "standing up" or "inclined" to the surface, and whether different adsorption sites are present. Once the adsorbate has been identified and its electronic orbitals defined, its geometry may be deduced from ARUPS measurements [92, 93].

In the following three Sections, we discuss case studies of the determination of molecular surface structure that illustrate the combined application of LEED and HREELS and our current ability to study molecules adsorbed at surfaces.

1. Structure of Adsorbed CO on the Rh(111) Surface

The HREELS spectra of CO chemisorbed on Rh(111) at 300 K as a function of exposure are shown in Figure 15 [94, 95]. At very low exposures (less than 0.1 L; 1 L = 1 Langmuir = 10^{-6} torr sec) only one peak at 2016 cm^{-1} is

observed in the C—O stretching (ν_{C-O}) region and no ordered LEED pattern is found. By comparison with the infrared spectra of relevant organorhodium compounds and with matrix isolated metal carbonyls, one can assign this loss to ν_{C-O} of a species at an atop site species. This peak shifts to higher frequency as the coverage is increased, due to one or several causes: local field effects, vibrational coupling, dipole-dipole interactions or a decrease in the metal-carbon backbonding due to the increased number of adsorbate molecules. The Rh—C stretching vibration (ν_{Rh-C}) for this linearly-bonded species does not shift from 468 cm^{-1} with increasing CO exposure. No other vibrations corresponding to Rh—C—O bending modes were observed in the specular direction. By using the dipole selection rule, one can conclude that the C—O bond is oriented perpendicularly to the surface.

At larger than 1.0 L CO exposures, a small shoulder near 1835 cm^{-1} appears. Again by comparison with relevant model compounds, one can

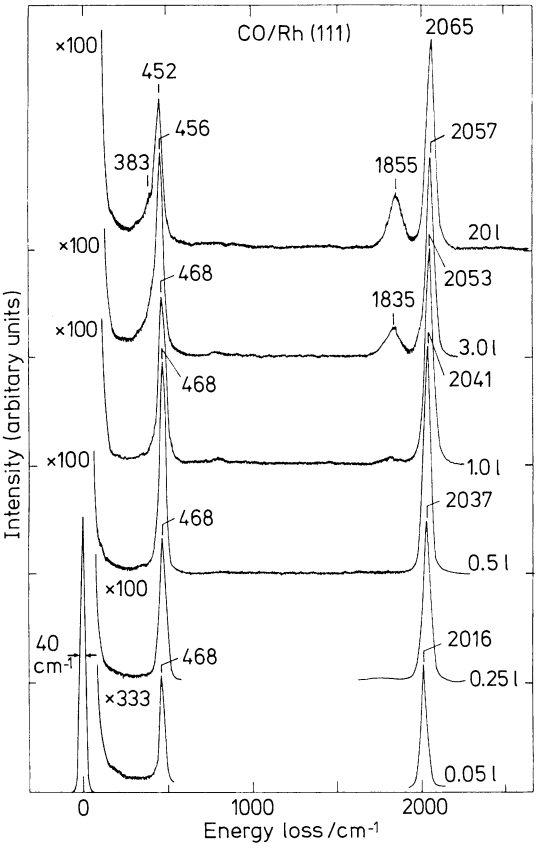

Figure 15. Vibrational spectra obtained by HREELS of CO chemisorbed on Rh(111) at 300 K as a function of CO exposure. The top spectrum represents a saturation coverage of CO under ultrahigh vacuum conditions. Reproduced with permission from ref. [95]

assign this peak to ν_{C-O} of a bridge-bonded species. This peak shifts to lower frequency with increasing CO exposure. By a CO exposure of 3.0 L, the ν_{Rh-C} loss peak broadens. The new low frequency shoulder appearing at about 380 cm^{-1} corresponds to ν_{Rh-C} of the bridge-bonded species. Again, the bridge-bonded species is oriented perpendicularly to the surface, since no bending modes are observed in the specular direction.

The vibrational spectra of CO chemisorbed on Rh(111) at 300 K with increasing background CO pressure (up to 10^{-3} Pa) show few changes with the increased CO coverage. The ν_{C-O} mode for the atop site shifts slightly higher as a function of coverage. A relative increase of the amount of bridge-bonded CO compared to CO in atop sites occurs. The ν_{C-O} mode due to the bridge-bonded species does not shift appreciably with increasing coverage.

Infrared spectroscopic studies on evaporated Rh films and on supported Rh cluster carbonyls of known molecular structure have also been made and analogous stretching frequencies in the 1800–2100 cm^{-1} region were observed. For Rh films, weak absorption peaks near 400–575 cm^{-1} were seen, indicative of Rh—C stretching and bending vibrations. Infrared studies [96] of highly dispersed Rh particles supported on Al_2O_3 showed a doublet at 2095 and 2027 cm^{-1}, and it was concluded that a gem dicarbonyl species of the form $Rh(CO)_2$ was formed in addition to atop and bridge-bonded species. No significant concentration of a gem dicarbonyl species was detected in the HREELS studies and it seems unlikely that these species would be formed in this case because of the high density of metal atoms on the Rh(111) surface that would lead to extreme crowding of CO molecules in the dicarbonyl configuration. Also, in infrared studies of Rh films, no $Rh(CO)_2$ species were observed, presumably again due to steric hindrance.

The chemisorption of CO on Rh(111) is completely reversible. No decomposition was detected under any of the conditions employed in the HREELS experiments ($p \leqq 1.3 \times 10^{-3}$ Pa CO, $T \leqq 600$ K), evidenced by no new Rh—C or Rh—O stretching vibrations.

We now turn to LEED crystallographic studies performed in our laboratory on the same CO adsorption system [97]. An interesting sequence of LEED patterns is observed as a function of CO coverage, as shown in Figure 16. The clean Rh(111) surface has a LEED pattern (Figure 16a) consisting of a hexagonal array of spots with the 3-fold symmetry characteristic of the ideal truncation of the unreconstructed bulk Rh lattice. With increasing CO coverage, a set of extra spots becomes visible that sharpen and reach maximum intensity at 1/3 monolayer coverage (Figure 16b): the corresponding pattern, which again is hexagonal with 3-fold symmetry, is labelled $(\sqrt{3} \times \sqrt{3})$ R30°, because the unit cell of the absorbate layer is enlarged by a linear factor $\sqrt{3}$ and rotated 30° with respect to the clean Rh(111) unit cell. At these coverages only one adsorption site is detected by HREELS, namely the atop site.

At near saturation coverages, the extra LEED spots split up in a complicated fashion, weaken and later reappear as shown in Figure 16c. By increasing the CO pressure in the vacuum chamber by several orders of magnitude, it

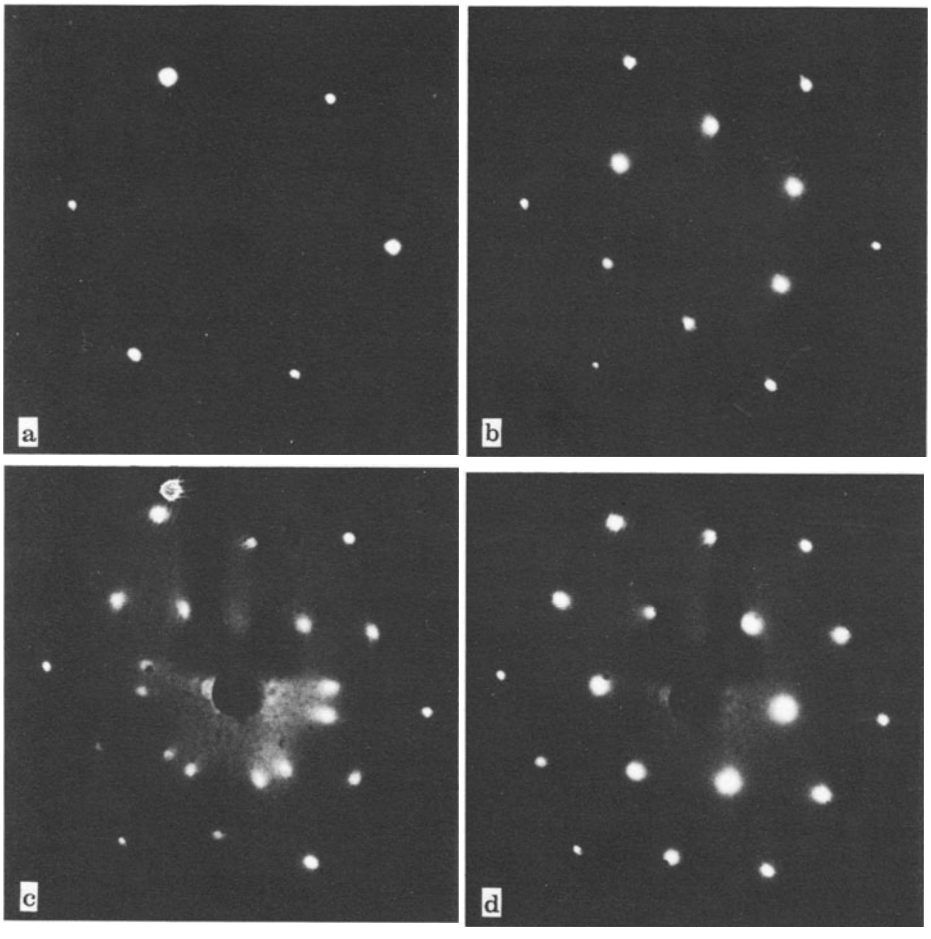

Figure 16. LEED patterns for CO adsorption on Rh(111): **a** clean Rh(111); **b** ($\sqrt{3} \times \sqrt{3}$) R30 pattern for 1/3 monolayer of CO; **c** "split (2×2)" pattern for between 1/3 and 3/4 monolayer of CO; **d** (2×2) pattern for 3/4 monolayer of CO

is possible to slightly increase the CO coverage and the end result is the (2×2) pattern seen in Figure 16d. The CO coverage at this stage is estimated to be 3/4 of a monolayer, corresponding to three molecules per (2×2) unit cell. At coverages just above the one corresponding to the ($\sqrt{3} \times \sqrt{3}$) R30° pattern, HREELS shows a loss peak growing in at the bridge-bonded CO frequency and this peak bridge-site frequencies and these continues to grow until the (2×2) pattern is achieved.

Both ordered CO structures, ($\sqrt{3} \times \sqrt{3}$) R30° and (2×2), were good candidates for a full LEED analysis, which would permit confirmation of the site assignment based on vibrational frequencies. A LEED analysis for the 1/3 monolayer structure [97] will be described first, and then the 3/4 monolayer structure determination [98] will be discussed.

In light of previous problems encountered in LEED studies of CO adsorption, particular attention was given to the surface cleanliness of the Rh(111) crystal, the LEED beam induced damage of the CO overlayer, and the optimal CO exposure values for the $(\sqrt{3}\times\sqrt{3})$ R30° structure. In the theoretical analysis of the measured I–V curves, a LEED formalism that includes multiple scattering was applied. The rhodium atoms were represented by a bulk band structure muffin-tin potential, which had been used successfully in other LEED work on clean Rh(111) to describe the manner in which electrons are scattered by the atoms. For the C and O atoms, Xα muffin-tin scattering potentials calculated for a NiCO cluster were chosen since these produced good LEED results on a nickel substrate.

Theory and experiment are compared through a set of R-factors (reliability factors) and their average, so as to quantify the comparison. While the final R-factor value for a given surface structure is obtained by averaging over all available diffracted beams with weights proportional to each beam's energy range, differences between R-factors for different beams can be exploited in the structure search. This is because different beams should simultaneously show minima when the correct surface structure is used, while with incorrect geometries it would be improbable to obtain this coincidence of minima.

In the first stage of the structural analysis, the clean Rh(111) surface was confirmed to have the ideal bulk structure. For the Rh(111) + $(\sqrt{3}\times\sqrt{3})$ R30° CO structural determination, four adsorption sites were analyzed: atop site, bridge site, and hcp and fcc hollow sites. The CO molecule was kept perpendicular to the surface in all cases. The hollow sites were easily ruled out by comparison of theoretical and experimental normal-incidence ($(\theta = 0°)$ I–V curves, while the bridge site was ruled out with off-normal incidence ($\theta \neq 0°$) I–V curves. The $\theta = 0°$ data produce a minimum average R-factor near the layer spacings (d_{RcH}, d_{CO}) = (0.201, 0.102) nm, while the $\theta = 10°$ and $\theta = 20°$ data produce minima at (0.1945, 0.1075) nm and (0.1945, 0.1085) nm, respectively. Averaging with weights proportional to the amount of data at each angle of incidence produces values of d_{Rh} = 0.195 ± 0.01 nm, and d_{CO} = 0.107 ± 0.01 nm, where the conventional uncertainty of LEED analyses is quoted. The structure of this surface is shown in Figure 17, as determined by LEED.

The R-factor contour plot around the minimum had an elongated elliptical shape with a major-to-minor axis ratio of up to ~4:1. This elongation

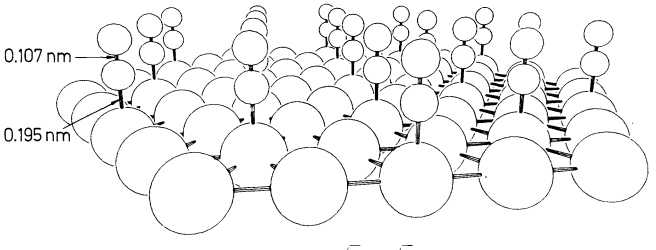

Figure 17. Structure of Rh(111) $(\sqrt{3}\times\sqrt{3})$R30° CO. Reproduced with permission from ref. [97]

implies an uncertainty in the carbon position, but not in the oxygen position, as can also be seen by the consistancy of the optimum Rh—O distances found at the three incidence directions (0.303, 0.302, and 0.302 nm at $\theta = 0$, 10, and 20°, respectively), while the C position varies by 0.007 nm.

The uncertainty in the carbon position may explain the slight discrepancy between the LEED results ($d_{RhC} = 0.195$ nm, and $d_{CO} = 0.107$ nm) and known Rh—C and C—O bond lengths in rhodium carbonyls, which range from 0.182 to 0.191 nm, and from 0.109 to 0.117 nm, respectively, according to a tabulation for terminal bonding in 10 different such carbonyl clusters [99]. In those clusters the Rh—O distance ranges from 0.296 to 0.304 nm. Thus the LEED determination puts the C atom somewhat far from the metal, but not the O atom.

The LEED result of top site adsorption for Rh(111) + ($\sqrt{3} \times \sqrt{3}$) R30°CO serves as a confirmation of the postulated correspondence in HREELS between adsorption site and vibrational frequency range for CO adsorbed on different metal surfaces. This confirmation is thereby extended to other than the fcc(100) substrate face, for which it was established previously with CO on Ni, Cu, and Pd(100). A summary of these results is included in Table 2. Note that the frequency ν_{C-O} for the Rh(111) + ($\sqrt{3} + \sqrt{3}$) R30° structure is closer to the frequency range associated with a bridge-bonded CO molecule than that for CO on Ni or Cu(100).

Such confirmations of the expected sites provide an important calibration of the vibrational techniques in the sense that the knowledge of the CO adsorption site at one coverage or on one crystal face can be used to determine, without the help of further LEED intensity analyses, the adsorption site on other substrate faces, at other coverages, or in disordered states.

LEED analysis of the (2 × 2) structure of CO on Rh(111) at 3/4 monolayer coverage has in turn confirmed the HREELS prediction that both bridge sites and top sites are occupied in that dense structure. The structure of Rh(111) + (2 × 2) 3CO is shown in Figure 18, as determined by LEED. This was a more complicated analysis, because three molecules fit in each unit cell and there were consequently more structural parameters to fit the experiment, a situation that LEED practitioners are only now learning to handle.

A general surface arrangement for this case might assume a hexagonal lattice of molecules (due to the dense packing), all oriented perpendicularly to the surface. However, this choice forces the atop-site molecules off the atop sites by 0.078 nm, which may not be the most favorable bonding geometry. The LEED intensity analysis indicates that, while the CO molecular axes are indeed essentially perpendicular to the surface (within about 10°) the atop-site molecules appear to move closer to the atop sites than illustrated (by about 0.025 nm), but not all the way because of steric hindrance. These "near-atop" molecules have a Rh—C bond length of 0.194 ± 0.007 nm (compared with 0.195 ± 0.01 nm in the atop-only ($\sqrt{3} \times \sqrt{3}$) R30° structure) with a Rh—C—O bond angle of 164 ± 10°, while the C—O bond length is 0.115 ± 0.01 nm (compared with 0.107 ± 0.01 nm in the atop-only structure). The bridge site molecules have a larger Rh—C bond length of

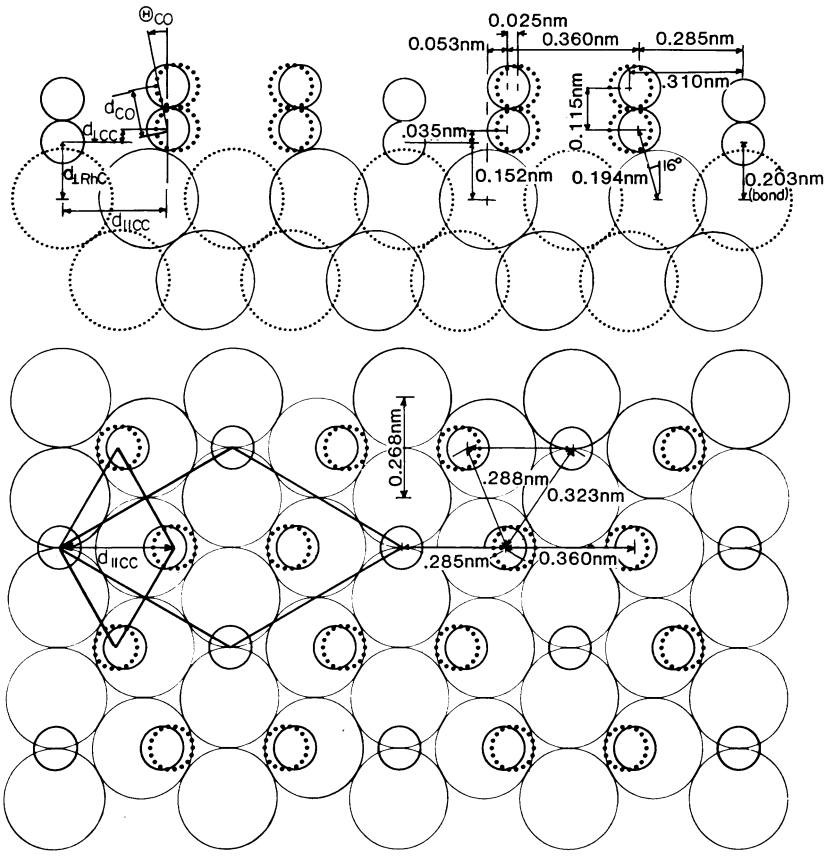

Figure 18. Structure of Rh(111) + (2×2) 3CO. The upper figure presents a side-view of the surface and the lower figure gives a top-view. The large circles represent Rh atoms (dotted—out of plane, full—in plane), and the small circles are either carbon or oxygen atoms (dotted—hexagonal mesh, full—measured positions). The five structural parameters that were varied in the LEED analysis are illustrated in the upper left corner. Reproduced with permission from ref. [98]

0.203 ± 0.01 nm, with again a C—O bond length of 0.115 ± 0.01 nm. These values are in good agreement with corresponding values found in rhodium carbonyl clusters [99], where atop site and bridge site molecules have Rh—C bond lengths of 0.182–0.192 nm and 0.200–0.208 nm, respectively, and C—O bond lengths of 0.109–0.117 nm and 0.114–0.117 nm, respectively.

In conclusion, by combining TDS, HREELS, and LEED analyses we can present a fairly complete picture of CO chemisorption on Rh(111). At very low exposures a single species is present on the surface located in an atop site (ν_{Rh-C} = 468 cm^{-1}, ν_{C-O} = 2016 cm^{-1}). As the coverage increases, the bonding to the surface becomes weaker and the TDS peak maximum shifts to lower temperatures [94, 100, 101]. This process continues until after approximately 0.5 L exposure where a $(\sqrt{3}\times\sqrt{3})$ R30° LEED pattern is seen

and all of the adsorbed CO molecules are in atop sites linearly bonded to individual rhodium atoms, with a Rh—C bond length of 0.915 ± 0.01 nm and a C—O bond length of 0.107 ± 0.01 nm. Above this coverage, a second C—O stretching vibration corresponding to a bridge-bonded species is observed (ν_{Rh-C} = 380 cm^{-1}, ν_{C-O} = 1855 cm^{-1}). A "split" (2×2) LEED pattern is seen indicating a loosely packed overlayer of adsorbate molecules. This overlayer structure compresses upon further CO exposure. Throughout this intermediate coverage regime there is a mixed layer of atop and bridge-bonded CO species, and we see a continuous growth of all HREELS peaks. Two peaks are also visible in the TDS spectra with a bridge-bonded CO having a 4 kcal/mole lower binding energy to the surface than the species located in the atop site. With a background pressure of $\sim 1.3 \times 10^{-4}$ Pa CO at 300 K, a (2×2) LEED pattern forms whose unit cell consists of three CO molecules, two atop and one bridged, in reasonable agreement with the 2:1 peak intensity ratio found in the HREELS spectra. LEED indicates that all CO molecules are still oriented nearly perpendicular to the surface in this dense (2×2) structure, with Rh—C bond lengths of 0.194 ± 0.01 nm and 0.203 ± 0.01 nm and CO bond lengths of 0.115 ± 0.01 nm and 0.115 ± 0.01 nm for near-atop and bridge site molecules, respectively.

2. *Structure of the Adsorbed Benzene Monolayer on Rh(111)*

Four different LEED patterns have been observed for benzene adsorption on Rh(111) at 240–395 K [102–106]. Most information is for $\begin{pmatrix} 3 & 1 \\ 1 & 3 \end{pmatrix}$ = c (2 $\sqrt{3}$ × 4) rect pattern (the "rect" notation indicates a rectangular unit cell with sides 2 $\sqrt{3}$ and 4 times the substrate surface lattice constant) and a $\begin{pmatrix} 3 & 0 \\ 0 & 3 \end{pmatrix}$ = (3 × 3) pattern. The LEED patterns and the geometry of the adsorbed monolayer for these structures are shown in Figure 19 and Figure 20, respectively [103]. The other observed patterns were $\begin{pmatrix} 3 & 3 \\ 2 & 2 \end{pmatrix}$ = (2 $\sqrt{3}$ × 3) rect and $\begin{pmatrix} 3 & 2 \\ 1 & 3 \end{pmatrix}$ = ($\sqrt{7}$ × $\sqrt{7}$) R 19.1°. The sizes of the four corresponding unit cells are 8, 9, 6 and 7, respectively, in terms of the number of surface Rh atoms included. The unit cells of size 7, 8, and 9 are compatible with known Van der Waals dimensions of flat-lying benzene molecules, assuming one molecule per cell; the (2 $\sqrt{3}$ × 3) rect unit cell contains two very crowded flat-lying molecules. The benzene molecules are known to lie flat from HREELS data [102, 106].

The c(2 $\sqrt{3}$ × 4) rect structure is stable up to about 370 K. At higher temperatures an irreversible order-order phase transition occurs to form the (3×3) structure. The (3×3) structure is stable to about 395 K, where it irreversibly disorders (just prior to the H_2 desorption peak in TDS). There are indications that the (3×3) structure might be stabilized by car-

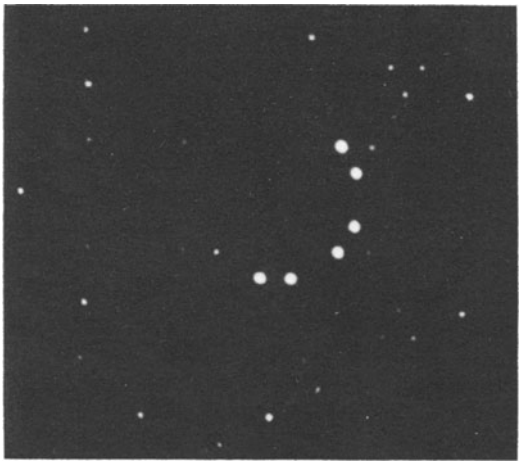

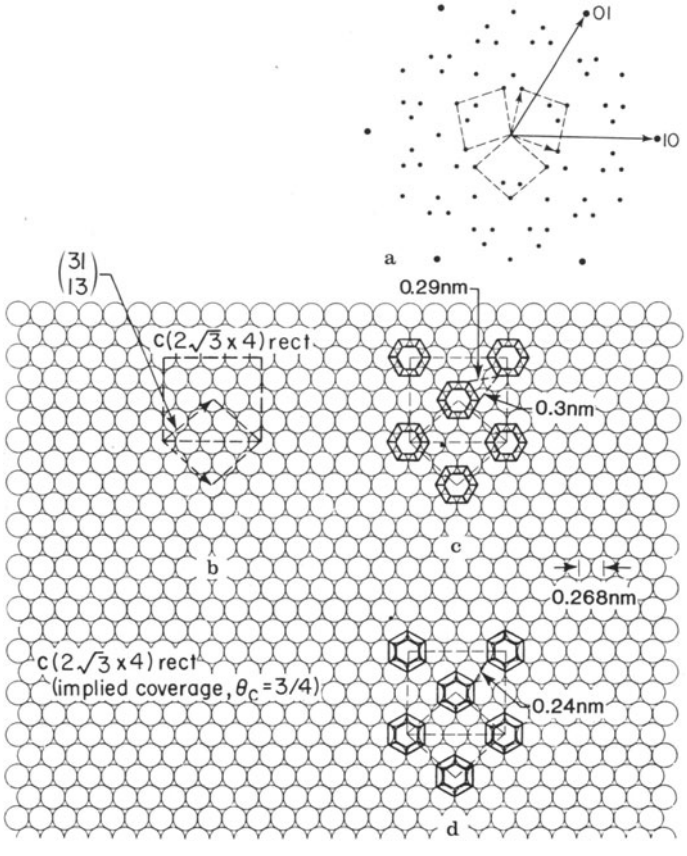

Figure 19. Rh(111) $+\begin{pmatrix} 3 & 1 \\ 1 & 3 \end{pmatrix} C_6H_6$ **a** LEED pattern at normal incidence at beam energy 50 eV: diffraction photograph at left; schematic diagram at right showing three unit cells in reciprocal space, corresponding to three domain orientations. **b** Real-space unit cell corresponding to the observed diffraction pattern, exhibiting the $\begin{pmatrix} 3 & 1 \\ 1 & 3 \end{pmatrix}$ unit cell and the centered rectangular $c(2\sqrt{3}\times 4)$ rect cell for one domain orientation. **c** and **d** Two possible models for benzene adsorption, differing by the azimuthal orientation of flat-lying molecules. The molecules are drawn as lines connecting C and H nuclei. The closest intermolecular distances are shown between H nuclei. Reproduced with permission from ref. [103]

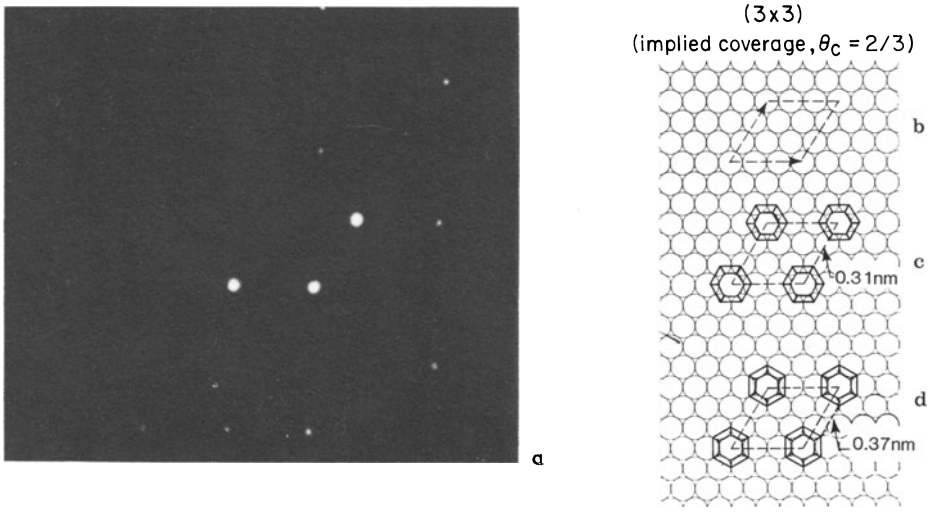

Figure 20. Rh(111) + (3×3) C_6H_6 **a** Photograph of LEED pattern at normal incidence at beam energy 50 eV. **b** Real-space unit cell corresponding to the observed pattern. **c** and **d** Two possible models for benzene adsorption, analogous to Figures 19c and 19d. Reproduced with permission from ref. [103]

bonaceous fragments resulting from partial benzene decomposition at the higher temperatures or from CO coadsorption.

TDS, using a 10 K/sec linear heating rate, shows two H_2 desorption states from a saturated surface: a peak at 413 K, due to decomposition of molecular benzene, and a broad state extending to about 700 K, due to subsequent dehydrogenation of the remaining hydrocarbon fragments. In addition, a small amount ($\leqq 20\,\%$) of molecular benzene desorption occurs prior to 415 K.

The existence of commensurate overlayer structures and the high desorption temperature of benzene on Rh(111) indicate strong metal-carbon bonding, which in the flat-lying geometry would involve the π-orbitals of the benzene ring. Strong bonding to the metal could distort the molecules: *e.g.*, C—C bond length expansions and C—H bond bending away from the surface might be expected in analogy with acetylene and ethylene adsorption on transition metals and with benzene structures in organometallic clusters. However, HREELS which will be discussed later, shows that this molecular distortion, if any, preserves a high symmetry of type $C_{3v}(\sigma_d)$ for both the $c(2\sqrt{3} \times 4)$ rect and (3×3) structures [102, 106].

By comparing measured and calculated LEED I–V curves, the detailed position of the adsorbed benzene molecules in the $c(2\sqrt{3} \times 4)$ rect and (3×3) structures have been analyzed [104, 105]. For both of these structures, about 960 structural models were investigated, differing in metal-molecule interlayer spacing, adsorption site, azimuthal orientation of the molecules about their six-fold axis, buckling, and planar distortions. In the $c(2\sqrt{3} \times 4)$ rect case, as shown in Figure 21, LEED calculations find that benzene is centered over a hcp hollow adsorption site (over a Rh atom in the second metal

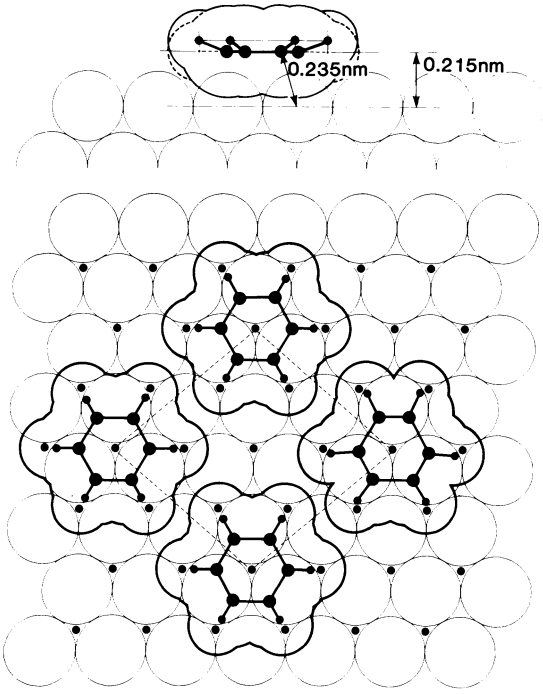

Figure 21. Optimal structure found for Rh(111) + c(2$\sqrt{3}\times4$) rect C_6H_6 (H positions are assumed), including Van der Waals radii of 0.18 and 0.12 nm for C and H, respectively. A unit cell is outlined in the bottom panel. The right-hand benzene molecule shows the preferred in-plane distortion (C—C bond lengths of 0.125 and 0.16 nm). The side view in the top panel includes possible CH bending away from the surface. Reproduced with permission from ref. [105]

layer); each of the three metal atoms around the hollow site would be bonded to two carbon atoms equally distant at about 0.235 $\pm$ 0.005 nm. This bonding corresponds to a planar (possibly distorted, as in Figure 21) C_6 ring with a metal-molecule layer spacing of 0.215 nm, similar to corresponding values in organometallic clusters containing aromatic rings. The symmetry of the adsorption site is $C_{3v}(\sigma_d)$. In this symmetry group, the symmetry planes of the Rh(111) substrate bisect the dihedral angles between the H atoms of the benzene ring. In the (3×3) case, no structural model has so far given satisfactory agreement between theory and experiment.

HREELS spectra for specular scattering are shown in Figure 22 [102]. These were taken following benzene adsorption on Rh(111) at 300 K to give a well-ordered c(2$\sqrt{3}\times4$) rect structure in LEED. The isotopic shifts observed for the spectra of C_6H_6 and C_6D_6 shown in Figures 22(A) and 22(B), respectively, allow for the identification of the losses at 345, 550, and 1420 cm^{-1} as two Rh—C and one C—C vibration frequencies, and those at 810, 1130 and 3000 cm^{-1} as C—H vibration frequencies. Strong bonding between the molecularly adsorbed benzene and metal occurs, as evidenced by the adsorption induced shifts of the C—H bending mode (from 673 cm^{-1} in the gas phase to 3000 cm^{-1}), but substantial rehydridization to an in the gas phase to 30000 cm^{-1}), but substantial rehydridization to an adsorbed cyclohexane-like species does not occur. From specular HREELS spectra, using the surface dipole selection rule and comparing infrared spectra of gas and liquid phase benzene, one can immediately conclude that

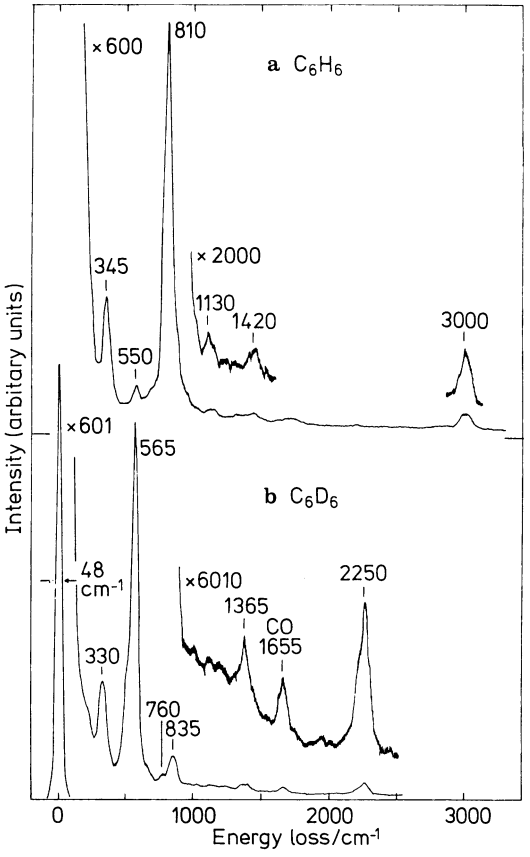

Figure 22. Vibrational spectra obtained by HREELS in the specular direction for saturation coverage of benzene chemisorbed on Rh(111) at 300 K which gives a $c(2\sqrt{3}\times 4)$ rect LEED pattern: (A) C_6H_6 (B) C_6D_6. The incident beam energy was 3.5 eV. Reproduced with permission from ref. [102]

the benzene molecule is adsorbed with the ring plane essentially parallel to the Rh(111) surface in the $c(2\sqrt{3}\times 4)$ structure, in agreement with LEED molecular-packing arguments. The most intense feature in Figure 22(A) is the 810 cm^{-1} loss corresponding to the out-of-plane C—H bending mode. The in-plane vibrational modes have very small intensities: 1130 cm^{-1}, C—H bend; 1420 cm^{-1}, C—C bend; and 3000 cm^{-1}, C—H stretch.

Structural information regarding the adsorption geometry and the symmetry of the adsorbed complex can be determined by comparing the number, frequency, and intensity of the dipole-active modes with the correlation table of the point group for the gas phase molecule. Adsorption of benzene with a symmetry group lower than C_{3v} can be ruled out, due to the small number of vibrational modes observed on-specular in Figure 22. Further refinement of the symmetry of the adsorbed complex is more difficult, since it has been observed that for adsorbed hydrocarbons the impact and dipole scattering in specular spectra are often of similar intensity. Thus, observation of a loss peak in the specular spectrum does not necessarily mean that the mode is dipole active.

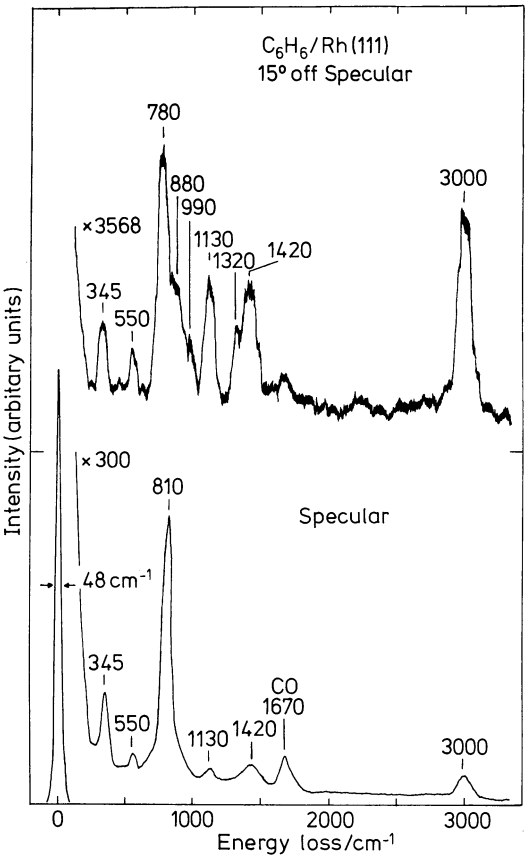

Figure 23. HREELS spectra obtained for specular and 15° off-specular scattering angles. The Rh(111) surface was saturated with benzene (C_6H_6) to produce the c(2$\sqrt{3}\times 4$) rect structure. Reproduced with permission from ref. [102]

Representative specular and off-specular spectra for benzene adsorbed to give the c(2$\sqrt{3}\times 4$) rect structure are shown in Figure 23. The off-specular spectrum was taken after a 7.5° rotation of the Rh(111) surface normal towards the analyzer, which corresponds to 15° off-specular scattering. This rotation caused a decrease in the elastic peak intensity by a factor of 170. The losses at 350 and 810 cm^{-1} were reduced by a factor of 10–15, while the other losses decreased in intensity by factors of 1.5–4. In addition, loss peaks can be identified in the off-specular spectra at 780, 880, 990 and 1320 cm^{-1}.

Except for the 350 and 810 cm^{-1} losses, the impact contribution to the observed intensity in specular scattering is substantial, and this makes the assignment of dipole-active peaks difficult. However, after a detailed angle-dependent study [106], we believe that all of the losses observed in the specular spectra have a non-zero dipole-active contribution.

The observation of the dipole-active peak at 1130 cm^{-1} (in-plane C—H bend, ν_{10} in the free molecule) leads to the conclusion that the adsorption site symmetry is $C_{3v}(\sigma_d)$. [106, 107] This result confirms the symmetry assignment from dynamic LEED calculations.

Ordered structures of adsorbed benzene have been observed on several metal surfaces: it is significant that they are all compatible with flat-lying benzene molecules, as we shall now show. The area of the benzene molecule in projection on its ring plane can be roughly estimated as that of the smallest rectangle that encloses it, using the Van der Waals ra ii of 0.12 nm: 0.5 nm^2. In the following cases the observed LEED pattern is consistent with one molecule per unit cell (the unit cell area A is given for comparison).

Ni(100) $c(4\times4)$—C_6H_6, [107] $A = 0.4960\ nm^2$,
Rh(111) $c(2\sqrt{3}\times4)$ rect-C_6H_6, $A = 0.4976\ nm^2$,
Rh(111) (3×3)—C_6H_6, $A = 0.5598\ nm^2$,
Ir(111) (3×3)—C_6H_6, [108] $A = 0.5766\ nm^2$,
Pd(100) $c(4\times4)$—C_6H_6, [93] $A = 0.6006\ nm^2$,
Ni(111) $(2\sqrt{3}\times2\sqrt{3})$ R30°—C_6H_6, [107] $A = 0.6443\ nm^2$,

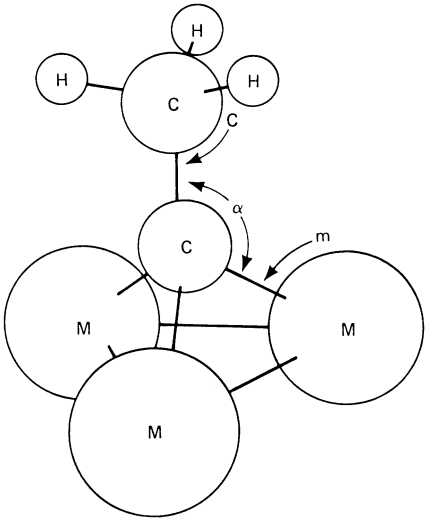

	C/nm	m/nm	r_M/nm	r_C/nm	α/deg
$Co_3(CO)_9CCH_3$	0.153	0.190	0.125	0.065	131.3
$H_3Ru_3(CO)_9CCH_3$	0.151	0.208	0.134	0.074	128.1
$H_3Os_3(CO)_9CCH_3$	0.151	0.208	0.135	0.073	128.1
Pt(111)+(2×2)CCH_3	0.150	0.200	0.139	0.061	127.0
Rh(111)+(2×2)CCH_3	0.145	0.203	0.134	0.069	130.2
H_3C-CH_3	0.154			0.077	109.5
$H_2C=CH_2$	0.133			0.068	122.3
$HC\equiv CH$	0.120			0.060	180.0

Figure 24. A model of the ethylidyne surface species. A comparison is made between the bond angles and distances found for this structure by LEED and those for corresponding organometallic compounds. r_C = carbon covalent radius; r_M = bulk metal atomic radius. Reproduced with permission from ref. [110]

On Pt(111) two benzene patterns have been observed that may be explained in terms of two flat-lying molecules per unit cell (half the unit cell area is therefore given here):

Pt(111) $(2\sqrt{3}\times 4)$ rect-2 C_6H_6, [110] $A/2 = 0.5316$ nm,

Pt(111) $(2\sqrt{3}\times 5)$ rect-2 C_6H_6, [110] $A/2 = 0.6645$ nm^2 .

It is of interest that no well-ordered incommensurate benzene structures have been reported in the literature or observed in our work on the various metal surfaces: this implies that the substrate-benzene interactions are strong compared with the benzene-benzene interactions.

3. *The Temperature Dependent Character of the Surface Chemical Bond: The Adsorption and Thermal Decomposition of Alkenes on Rh(111) and Pt(111) Surfaces*

Molecular adsorption of ethylene occurs at low temperatures on metal surfaces, at less than 240 K on Rh(111) and 280 K on Pt(111). The adsorbed molecules give no ordered structures, *i.e.*, no well-defined LEED patterns, but have been shown by UPS and HREELS to be bonded parallel to the metal surface and significantly rehydridized compared to the gas phase. Approximately sp^3 hybridization of the carbon atom results, while strong di-σ bonds to the metal atoms are formed [91].

We have the most detailed information on the structure of hydrocarbon monolayers that are formed from partially dehydrogenated alkenes [110]. These species form ordered overlayers and can be studied by LEED.

The best understood system is the simplest one, that of ethylidyne [111, 112]. This alkylidyne species, which is shown in Figure 24, has a carbyne carbon atom closest to the surface that is bound very strongly with a multiple metal carbon bond which is 0.02 nm shorter than the covalent distance of 0.22 nm. The carbon-carbon bond is stretched to a single bond and the methyl group extends essentially perpendicular to the surface. Figure 24 shows the ethylidyne surface structure with its interatomic distances and bond lengths, and compares these with organometallic cluster compounds of similar type. The cluster and adsorbed surface species have very similar structures, as shown. It is interesting, however, that the ethylidyne adsorption

Table 3. Comparison of the vibrational frequencies (cm^{-1}) of the ethylidyne surface species formed on Rh(111) [115] with those of the ethylidyne cluster compound [113]

Assignment	$CH_3CCo_3(CO)_9$	CH_3C—Rh(111)
$\nu_{as}(CH_3)/\nu_{as}(CD_3)$	2930(m)/2192(w) e	2920(vw)/2178(vw) e
$\nu_s(CH_3)/\nu_s(CD_3)$	2888(m)/ ----a_1	2880(w)/2065(vw) a_1
$\delta_{as}(CH_3)/\delta_{as}(CD_3)$	1420(m)/1031(w) e	1420(vw)/ ----e
$\delta_s(CH_3)/\delta_s(CD_3)$	1356(m)/1002(vw) a_1	1337(s)988(w) a_1
ν_{cc}	1163(m)/1182(ms) a_1	1121(m)/1145(m) a_1
$\varrho(CH_3)/\varrho(CD_3)$	1004(s)/828(s) e	972(vw)/769(vw) e
$\nu_s(MC)$	401(m)/393(m) a_1	435(w)/419(w) a_1

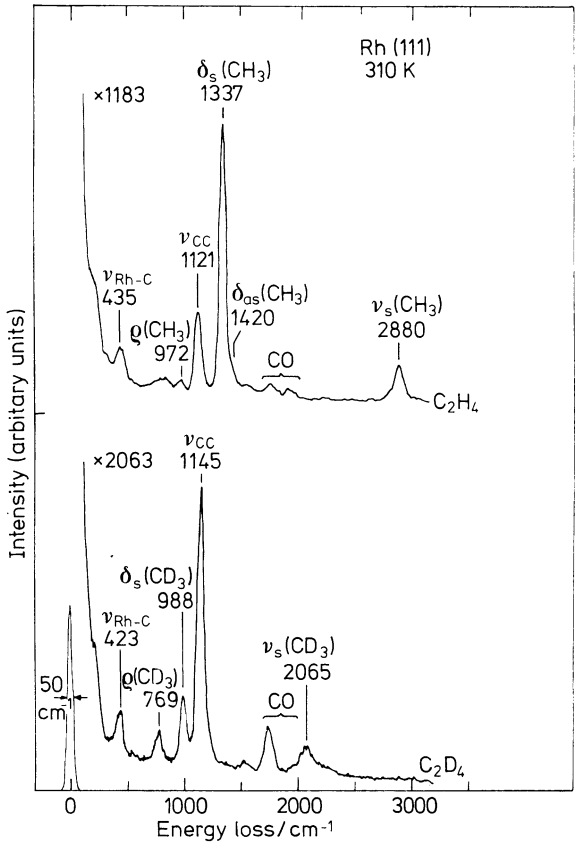

Figure 25. HREELS spectra of the ethylidyne surface species formed after 10L exposure of C_2H_4 (top) or C_2D_4 (bottom) to Rh(111) at 310 K. Spectra were recorded for specular reflection at an incident beam energy of 2.5 eV

site is the hcp hollow site on Rh(111) [112] and the fcc hollow site on Pt(111) [111].

Further evidence of the similarity of cluster compounds and surfaces containing ethylidyne is given by vibrational spectroscopy. In fact, one of the major factors that brought about agreement among surface scientists on the correct identification of this species was the close correlation between HREELS spectra of the surface species and the infrared spectra (including a normal mode analysis) of an ethylidyne containing cluster compounds, $CH_3CCo_3(CO)_9$ [113]. This correlation for Rh(111) is shown in Table 3. The HREELS spectra for the ethylidyne species is almost the same on Rh(111) [114, 115], Pt(111) [116], and Pd(111) [117] surfaces, and is shown

Figure 27. Vibrational spectra obtained by HREELS for a series of alkenes exposed to saturation coverage on Rh(111) at 310 K. Spectra were recorded for specular reflection at an incident beam energy of 2.5 eV ▶

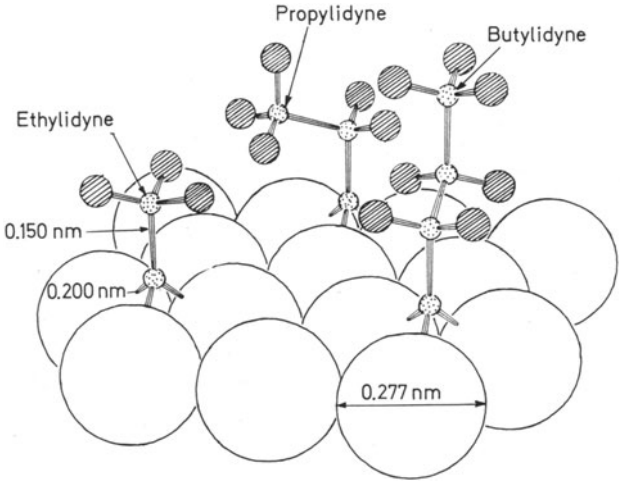

Figure 26. Alkylidyne (C_nH_{2n-1}) species are produced on the Pt(111) surface after alkene (C_nH_{2n}) adsorption at 300 K. Large circles represent top-layer Pt atoms, dotted circles indicate carbon atoms, and slashed circles are hydrogen atoms. Reproduced with permission from ref. [110]

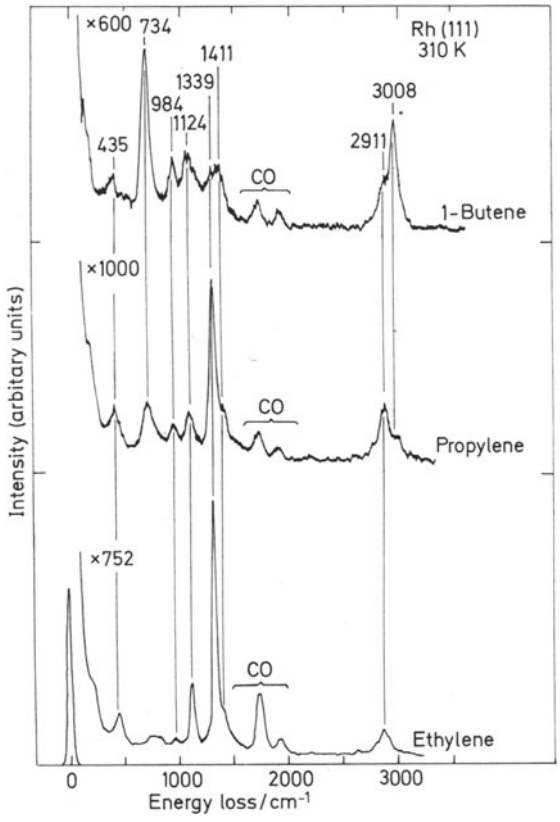

in Figure 25 for the case of Rh(111) [115]. Other evidence, such as results from TDS studies, supports the LEED and HREELS assignments.

Figure 26 shows the surface structures as they were determined by LEED for the stable alkylidyne species formed after ethylene, propylene, and 1-butene adsorption and dehydrogenation on Pt(111) surfaces [110]. These assignments were made mainly on the basis of closely-related LEED patterns and *I–V* curves for ethylene, propylene, and 1-butene adsorption on Pt(111). HREELS data support this conclusion [115, 119]. The alkyl group in these structures is away from the surface and appears to be rotating freely, except at high coverages where this group is "locked-in" in a periodic fashion to give rise to new diffraction features.

I–V curves obtained for the (2×2)spots after propylene exposure at room temperature on Rh(111) were also nearly identical to those for the (2×2) ethylidyne structure on this surface. However, in this case, HREELS spectra show that the propylene carbon skeleton is no longer intact — there is fragmentation to ethylidyne and C_xH species. Figure 27 shows results of an HREELS study of hydrocarbon monolayers formed by exposure of ethylene, propylene, and 1-butene to Rh(111) at 300 K [115]. Exposure of these gases at 300 K (as opposed to 230 K exposure, followed by annealing, as in previous

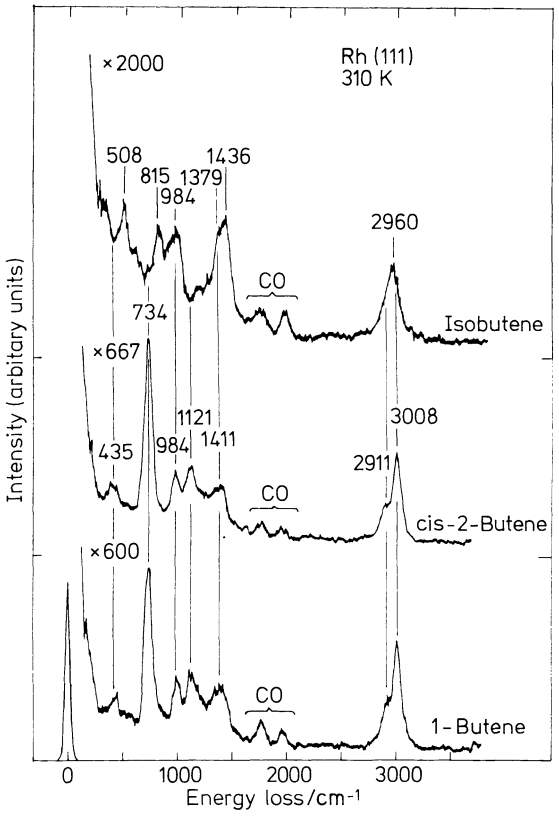

Figure 28. HREELS spectra for butene isomers adsorbed on Rh(111) at 310 K. Spectra were recorded for specular reflection at an incident beam energy of 2.5 eV

LEED studies) does not lead to well-ordered structures in LEED, but at least for ethylidyne, the surface species are the same. The propylene HREEL spectrum is similar to that for ethylidyne except for new features at 734 and 3008 cm^{-1} which are attributed to CH or C_2H fragments [115]. The 1-butene spectrum has also been tentatively assigned as a mixture of CH or C_2H fragments and propylidyne species resulting from carbon-carbon bond breaking between C_1 and C_2 analogous to the propylene fragmentation. Investigations are in progress to see if propylene and 1-butene form alkylidyne.

Figure 28 shows the HREELS spectra following exposure of three butene isomers to Rh(111) at 300 K [115]. The spectra reveal that 1-butene and 2-butene are isomerized to give the same surface species. Isobutene, on the other hand, forms a different surface species.

It is clear that HREELS can be used successfully to study even large adsorbed hydrocarbons. However, further HREELS studies are required (and are in progress) of the *ordered* hydrocarbon monolayers. Detailed off-specular HREELS spectra should be obtained on these other structures as in the case of ethylidyne to provide more conclusive assignments of these structures.

When hydrocarbon molecules, such as ethylene, propylene and butene, are adsorbed on transition metal surfaces and then the surface is heated, all but a few percent of the intact molecules will dehydrogenate rather than desorb. Hydrogen evolution is detected in the thermal desorption spectra

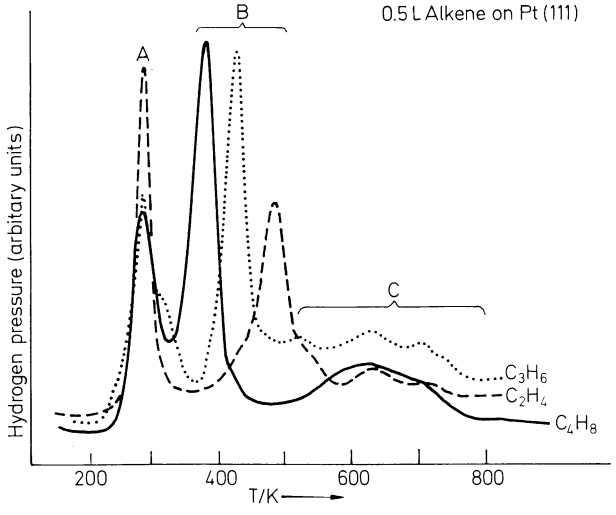

Figure 29. Thermal desorption spectra recorded for saturation coverages after alkene (C_2H_4, C_3H_6, 2-C_4H_8) adsorption on the Pt(111) surface. Peak (A) represents H_2 desorption at the alkene to alkylidyne conversion temperature; peak (B) indicates alkylidyne fragmentation accompanied by more H_2 desorption; and peak (C) represents graphite formation with complete dehydrogenation of the hydrocarbon overlayer. The heating rate in TDS was 7–14 K s^{-1}. Reproduced with permission from ref. [110]

for these molecules. For example, thermal desorption spectra taken after alkene adsorption on Pt(111) are shown in Figure 29. There are well-defined peaks indicating maximum rates of hydrogen desorption from the surface at well-defined temperatures. Sequential C—H bond breaking is characteristic of most organic molecules on metal surfaces. The thermal decomposition of alkylidyne surface species leads to the formation of mainly CH and C_2H species on the surface [115]. The fragmentation chemistry can be well characterized for these molecules by HREELS, as indicated by Figure 30.

The fragments that stay on the surface appear to be stable in a temperature range where the catalytic activity of the transition metals are the greatest.

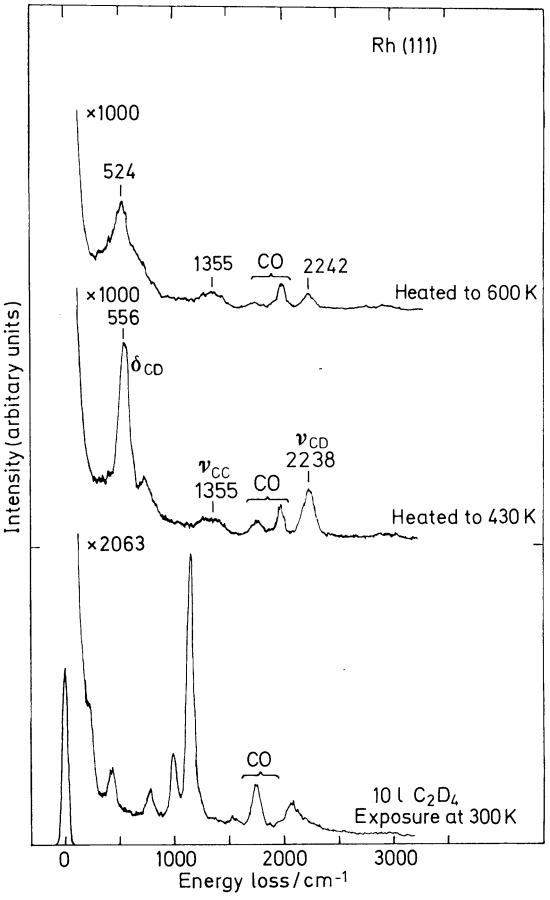

Figure 30. Thermal decomposition of the deuterated ethylidyne surface species on Rh(111) as studied by HREELS (specular scattering). TDS of this surface is similar to that shown in Figure 29 for C_2H_4 adsorbed on Pt(111), but with a D_2 peak at 430 K on Rh(111). A significant decomposition rate occurs at 410 K and HREELS shows the formation of primarily surface CH and C_2H species. The assignment of the adsorbed CH and C_2H species is confirmed by comparison with infrared spectra of relevant organometallic cluster compounds. These surface species are stable to at least 600 K. Above 800 K, all hydrogen is removed from the surface

Carbon-14 labeling techniques indicate very long residence times of these carbonaceous fragments as compared to turnover times for hydrocarbon conversion reactions. Thus, the carbon fragments are permanent fixtures of the catalytically active transition metal surface. What is the role of these carbonaceous fragments during catalysis? This question is under intense investigation. It appears that the hydrogen contained in these fragments readily exchanges with the incoming adsorbed molecules or surface intermediates on a time scale much shorter than the turnover rates of most reforming reactions. The picture that arises to explain the importance of these carbonaceous deposits emphasizes their role for hydrogen storage. Hydrogen that must be provided to surface intermediates before they can desorb is likely to be provided by these carbonaceous fragments. As long as hydrogen exchange and transfer is available to the surface intermediates, the catalytic activity of the transition metals is maintained. As soon as the carbonaceous deposits completely dehydrogenate at elevated temperatures by forming a graphitic overlayer, the catalytic activity ceases, and the carbonaceous layer becomes a catalyst poison.

For a given transition metal surface, the nature of the carbon fragments formed by thermal decomposition are similar regardless of what organic molecules were used during the initial stages of adsorption and decomposition. For example, the fragmentation of benzene on Rh(111) above 430 K appears very similar in HREELS to the results for alkylidyne decomposition above 430 K on Rh(111) [115].

Figure 31 shows the results of a theoretical calculation of the location of the various carbonaceous fragments on metal surfaces [118]. These extended-Hückel calculations find that the carbon in such fragments always prefer tetrahedral bonding. Thus, a CH fragment would occupy a three-fold site, a CH_2 fragment a two-fold site, and a CH_3 fragment a one-fold site. Although experimental confirmation of this model is lacking so far, it would

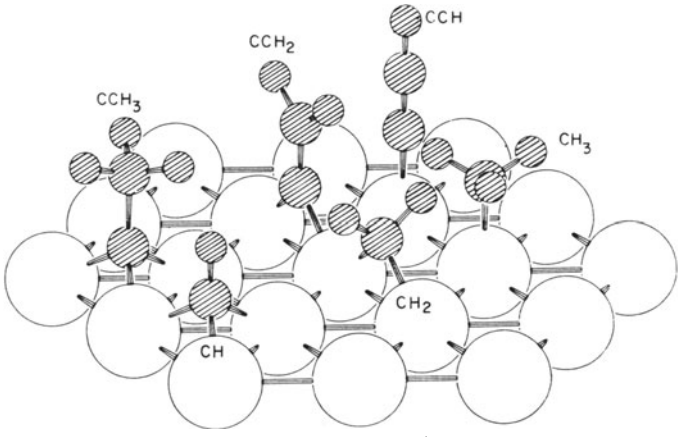

Figure 31. Preferred adsorption sites of CH, CH_2, CH_3, CCH_3, CCH_2, and CCH on Pt(111). Sphere radii have no physical significance. Reproduced with permission from ref. [118]

indicate that upon sequential hydrogenation, the fragment changes sites, thereby freeing those sites that were occupied and making them available to adsorb new, incoming molecules.

6. Future Directions in Surface Structural Determinations

There is intense research currently in the determination of surface structure. Advances in our knowledge of surface structural chemistry will obviously come with the increasing amount of data that is available. New techniques that were mentioned in Section IV are providing useful complementary information on systems studied by LEED and HREELS, and in addition are allowing studies of surface structures that can not be done with the latter two techniques. The development of these and newly devised techniques will continue to enlarge and improve the data base on surface structure. In addition, advances in the state-of-the-art LEED and HREELS experiments are occurring.

Large computers are making it possible now to run dynamical LEED calculations for more complex surface structures. Also, larger unit cells can now be handled efficiently. A powerful calculational LEED scheme called Beam Set Neglect [105] has also been introduced for superlattices with unit cells of any size. This scheme can also be applied to disordered systems removing the traditional requirement of periodicity. More data from LEED experiments that study disordered systems and island formation, by looking at the diffuse background intensity and the lateral profiles of the LEED spots, will be valuable. The rapid increase in the number of groups with low intensity (nanoampere beam current) LEED instruments should produce new, reliable information on sensitive organic molecules adsorbed on surfaces. Several of these instruments also have very large instrumental transfer widths (100–1000 nm) that allow studies of the long-range order on that scale: this is important for investigating island formation and phase transitions.

The usual operating resolution in HREELS has dropped by a factor of two in recent years, from 80–90 cm^{-1} to 30–50 cm^{-1} currently. This is still larger than the inherent linewidth of most adsorbed species, but enables the study of adsorption and bonding on heterogeneous surfaces (*e.g.*, stepped and alloy surfaces), atomic and molecular coadsorption, and more complicated hydrocarbon structures. Also, work is underway in developing a time-resolved HREELS technique to study surface kinetics. Better understanding of the scattering mechanism in HREELS has recently allowed more detailed information to be obtained. Two examples are the separation of dipole-dipole and other vibrational coupling effects from chemical bonding shifts in vibrational spectra and detailed angular studies of impact scattering from adsorbed monolayers.

Of course, one of the main goals of future structural chemistry research is to extend these studies across the Periodic Table, and correlate the data with atomic and electronic structure. New materials need to be studied, *e.g.*, carbides, nitrides, sulfides, carbonates, alloys, mixed oxides, and rare earth

compounds. Data on large sets of similar organic molecules adsorbed on the same solid surface should be obtained. Studies of organometallic cluster analogs of surface species on transition metal surfaces are important. Most important is to continue the close coupling of structural studies to applications of surface chemistry, *e.g.* corrosion, lubrication, coatings, and catalysis.

7. Implications to Catalysis: The Structure Sensitivity of the Surface Chemical Band

When carbon monoxide, hydrogen, or other small molecules are adsorbed on single crystal surfaces with various atomic structures, thermal desorption studies clearly indicate changes in the surface chemical bond with atomic locations. Figure 32 shows thermal desorption of H_2 from a (111) surface, (557) stepped surface, and a (12, 9, 8) kinked platinum surface. One peak is observed from the (111) surface, indicating rather uniform site adsorption for atomic hydrogen. From a stepped surface there are two peaks, indicating that at a step the molecules are bound more strongly and desorb at a higher temperature. From a kinked surface, there are three desorption peaks indicating that hydrogen adsorbs on terraces, at steps, and on kinks with different binding energies.

Figure 33 shows the desorption of carbon monoxide from a stepped surface of platinum at different coverages. At low CO coverages, the step sites are filled first and adsorption occurs only at these sites. When all the step sites are occupied (saturated), adsorption continues on terraces where the

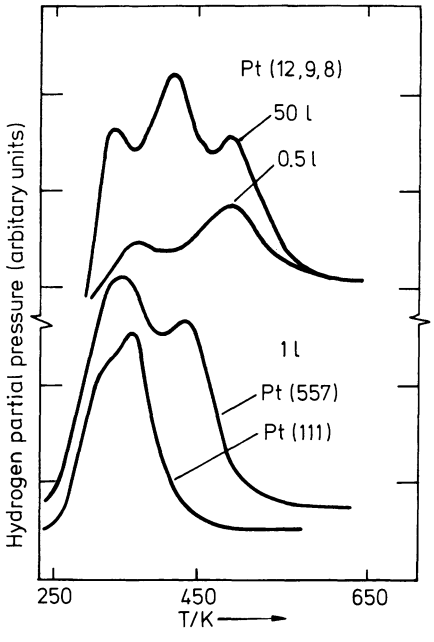

Figure 32. Thermal desorption spectra for hydrogen chemisorbed on flat Pt(111), stepped Pt(557), and kinked Pt(12, 9, 9) crystal surfaces

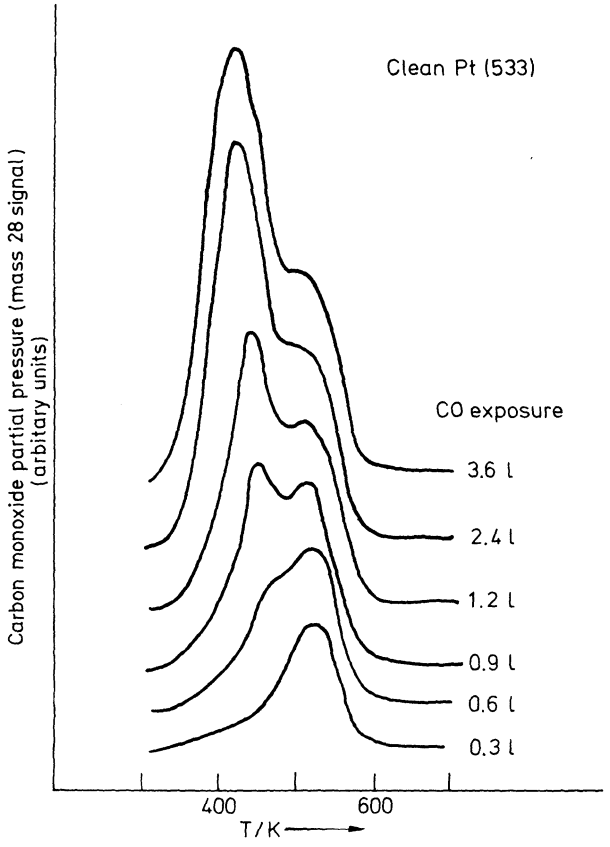

Figure 33. Thermal desorption spectra for CO chemisorbed on the stepped Pt(533) crystal surface with increasing CO coverage

Table 4. Binding states for CO on various platinum surfaces

Plane	Desorption Energies/kJ mol^{-1}
Pt(111)	124
	95
Pt(110)	109
	83
Pt(100)	134
	122
	111
	99
Pt(210)	*152*
	114
Pt(211)	147
	114

binding is weaker. This sequential filling of adsorption sites, starting with the higher energy adsorption site, is a common feature of the surface chemistry of adsorbates with increasing coverage. The diffusional mobility of atoms and molecules on the surface is usually adequate to assure that they

will find the site of highest binding energy to adsorb. It also reflects a definite influence of the local atomic structure on the chemical bonding of adsorbed species. Table 4 shows values for the heats of adsorption obtained for carbon monoxide on various platinum surfaces. The highest and the lowest binding energy sites are different by more than 50 kJ mol^{-1}, indicating a great diversity of chemical bonding with atomic surface structure. There is not one type of chemical bond between an adsorbed molecule and a given solid surface. There are many binding states whose strength depends on the local atomic structure.

Alterations of atomic structure can be obtained by depositing a second component metal on metal surfaces. When silver or copper is deposited on stepped surfaces of platinum, the second metal preferentially occupies the terrace sites. As a results, adsorption on terraces is impeded while step

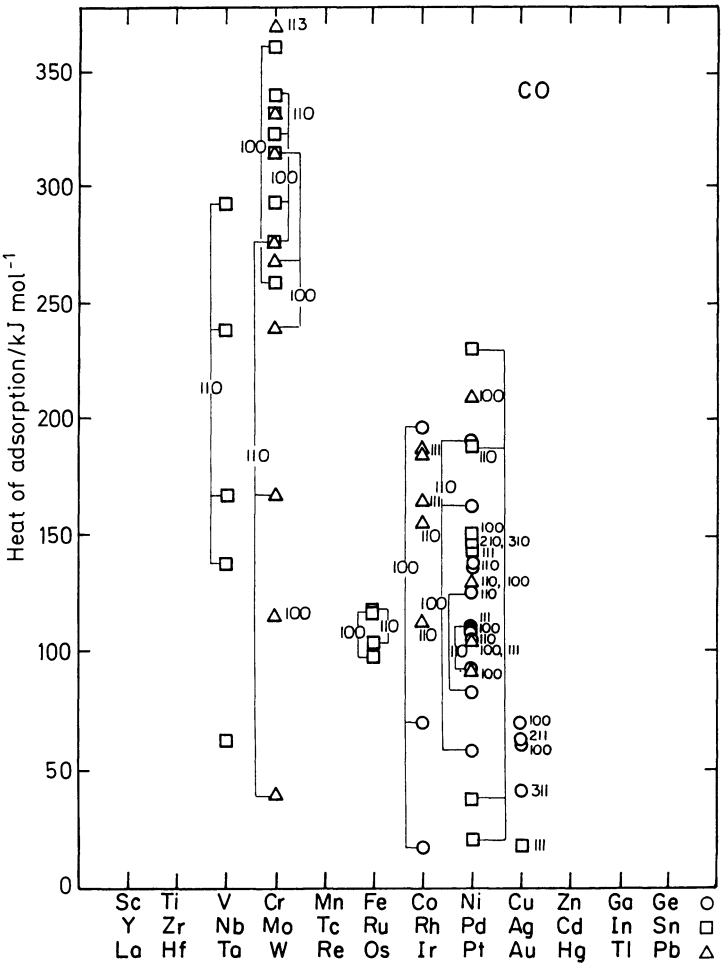

Figure 34. Heats of adsorption of CO on single-crystal surfaces of transition metals

adsorption continues unchanged. As a result, changes in the ratio of molecules in these different sites can be manipulated. Studies of similar systems will be likely to reveal new surface chemistry.

Over the past ten years a large body of data on heats of adsorption has been obtained from single crystal surfaces. This allows one to determine how the heat of adsorption varies across the Periodic Table. Figure 34 shows the variation of the heat of adsorption for single crystal surfaces adsorbing carbon monoxide. There is a very large variation of binding energies for a given solid surface depending on its atomic structure, and there is a definite trend of weaker chemical bonding as one goes from left to right across the transition metal series in the Periodic Table. When the same heat of adsorption information was obtained using polycrystalline surfaces, which average over the various binding sites that are all present on a given surface, a smoother curve is obtained and the declining heat of adsorption trend from left to right in the Periodic Table is readily visible. This is shown in Figure 35. In Figure 36 and 37, the same data is obtained for the hydrogen heat of adsorption across the Periodic Table for single crystal and polycrystalline surfaces, respectively. There is little detailed theoretical understanding of the reasons for these trends, although there have been numerous attempts to explain this phenomenon. The degree of overlap of the molecular or atomic orbitals of adsorbates with the density of states of the metal determines the nature of electron transfer into bonding and antibonding orbitals and determines the strength of the surface chemical bond. Theoretical scrutiny of this phenomenon is necessary and fruitful to understand the nature of the surface chemical bond of small atoms and molecules in more detail.

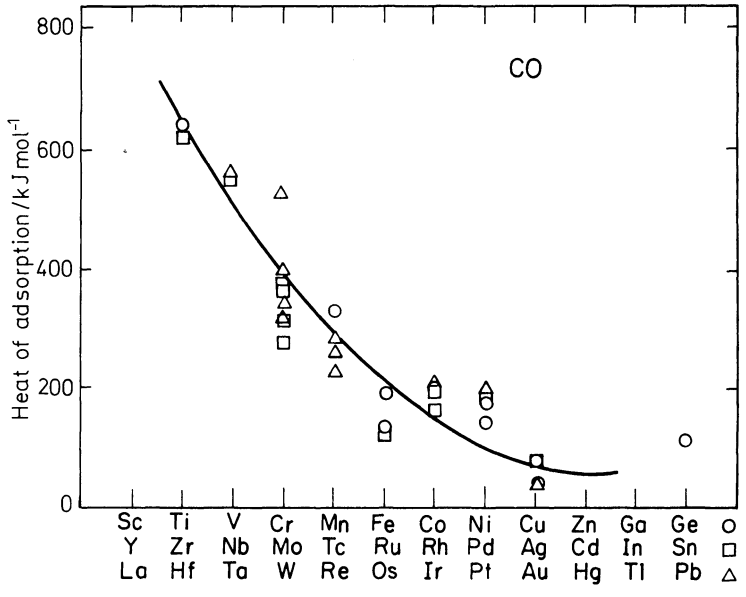

Figure 35. Heats of adsorption of CO on polycrystalline transitionmetal surfaces

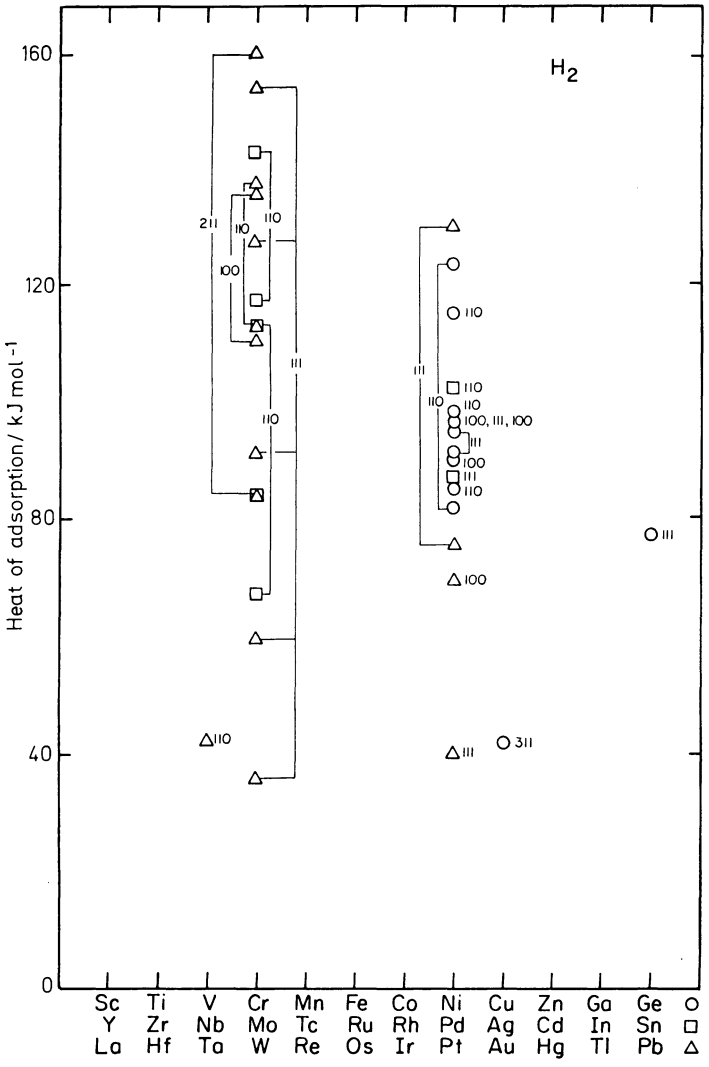

Figure 36. Heats of adsorption of hydrogen on single-crystal surfaces of transition metals

The physical picture that emerges from these surface studies is one of the predominance of surface structure-sensitive, localized bonding. An atom may adsorb on a high symmetry three-fold, bridge or two-fold, or on an atop or one-fold site. In each of these sites, the bonding strength may be different from that in other sites. Of course, in the presence of atomic steps and kinks, there are even more sites with different structures that may further change the local chemical bond. Thus, the localized bonding that involves an adsorbate atom or molecule and the nearest neighbor surface atoms indicates cluster-like surface chemical bonding, that describes well the structural and chemical characteristics of the surface adsorbate-substrate systems. Because

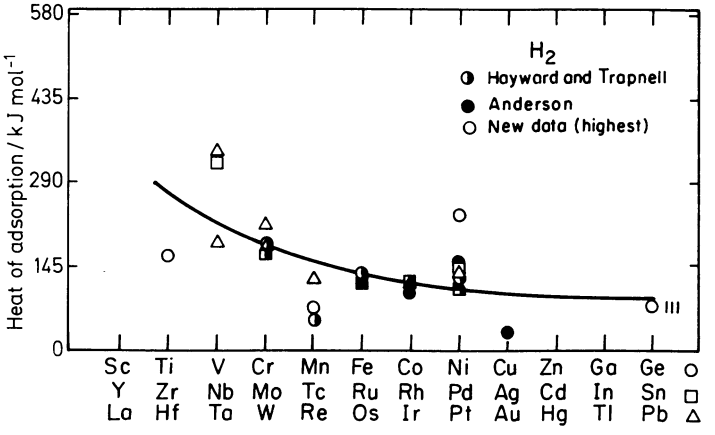

Figure 37. Heat of adsorption of hydrogen on polycrystalline transitionmetal surfaces. Data from: D. O. Hayward and B. M. W. Trapnell, *Chemisorption*, Butterworths, London, 1964; J. K. Anderson (ed.), *Chemisorption and Reactions on Metallic Films*, Academic, New York, 1971; I. Toyoshima and G. A. Somorjai, Catal. Rev. — Sci. Eng. *19* (1), 105 (1979)

of the structural richness of each surface, the nature of the surface chemical bond reflects the same diversity and complexity.

Over the past ten years, there have been great advances in our understanding of the nature of the surface chemical bond and the structure of adsorbed atoms and molecules on surfaces. We have briefly reviewed some results of studies, mostly by LEED and HREELS. As these and other techniques become more widely applied, the increased availability of experimental data will further accelerate the rate of development of surface chemistry and its applied subfields, catalysis among them.

Acknowledgement

We wish to thank Dr. M. A. van Hove for his many valuable discussions. One of us (BEK) would like to acknowledge support by the Miller Research Institute, University of California, Berkeley. This work was supported by the Director, Office of Energy Research, Office of Basic Energy Sciences, Materials Sciences Division of the U.S. Department of Energy under Contract DE-AC03-76SF00098.

8. References

1. Wood, E. A.: J. Appl. Phys. **35**, 1306 (1964)
2. Somorjai, G. A., Van Hove, M. A.: Adsorbed Monolayers on Solid Surfaces, Structure and Bonding, Vol. **38**. Berlin, Heidelberg, New York: Springer 1979
3. Ertl, G., Küppers, J.: Low Energy Electrons and Surface Chemistry. Weinheim: Verlag Chemie 1974
4. Heugler, M.: Surf. Sci. **19**, 159 (1970)

5. Laramore, G. E., Houston, J. E., Park, R. L.: J. Vac. Sci. Technol. **10**, 196 (1973)
6. Jagodzinski, H., Moritz, W., Wolf, D.: Surf. Sci. **77**, 233 (1978)
7. Ertl, G., Schillinger, D.: J. Chem. Phys. **66**, 2569 (1977)
8. Pendry, J. B.: Low Energy Electron Diffraction. New York—London: Academic Press 1974
9. Van Hove, M. A., Tong, S. Y.: Surface Crystallography by LEED. In: Springer Ser. Chem. Phys. **2**. Berlin, Heidelberg, New York: Springer 1979
10. Tong, S. Y.: A Review of Surface Crystallography by Low-Energy Electron Diffraction. In: Electron Diffraction 1927–1977. Dobson, P. J., Pendry, J. B., Humphreys, C. J. (eds.). London: The Institute of Physics, Bristol 1978, pp. 270–280
11. Van Hove, M. A.: Surface Crystallography and Bonding. In: The Nature of the Surface Chemical Bond. Rhodin, T. N., Ertl, G. (eds.). Amsterdam—New York—Oxford: North Holland 1979, pp. 275–312
12. Heinz, K., Muller, K.: LEED Intensities-Experimental Progress and New Possibilities of Surface Structure Determination. In: Structural Studies of Surfaces, Springer Tracts in Modern Physics, Vol. **91**. Berlin, Heidelberg, New York: Springer Verlag 1982, pp. 1–53
13. Ibach, H., Mills, D. L.: Electron Energy Loss Spectroscopy and Surface Vibrations. New York: Academic Press 1982
14. Sexton, B.: Appl. Phys. **A26**, 1 (1981)
15. Thiry, P. A.: J. Electron Spectrosc. Relat. Phenom. **30**, 261 (1983)
16. Froitzheim, H., Ibach, H., Lehwald, S.: Rev. Sci. Instrum. **46**, 1325 (1975)
17. Evans, E., Mills, D. L.: Phys. Rev. **B5**, 4126 (1972)
18. Ibach, H.: Surf. Sci. **66**, 56 (1977)
19. Evans, E., Mills, D. L.: Phys. Rev. **B5**, 4126 (1971)
20. Newns, D. M.: Phys. Lett. **60A**, 461 (1977)
21. Persson, B. N. J.: Solid State Commun. **24**, 573 (1977)
22. Ibach, H., Bruchmann, D.: Phys. Rev. Lett. **44**, 36 (1980)
23. Froitzheim, H., Ibach, H., Lehwald, S.: Phys. Rev. Lett. **36**, 1549 (1976)
24. Katz, J. E., Davies, P. W., Crowell, J. E., Somorjai, G. A.: Rev. Sci. Instrum. **53**, 785 (1982)
25. Cabrera, A. L., Spencer, N. D., Kozak, E., Davies, P. W., Somorjai, G. A.: Rev. Sci. Instrum. **53**, 20 (1982)
26. Menadue, J. F.: Acta Cryst. **A28**, 1 (1972)
27. Maserd, N., Kinniburgh, C. G., Pendry, J. B.: J. Phys. **C10**, 1 (1977)
28. Aberdam, D.: Electron Diffraction in the Medium-Energy Range. In: Electron Diffraction 1927–1977. Dobson, P. J., Pendry, J. B., Humphreys, C. J. (eds.). London: The Institute of Physics, Bristol 1978, pp. 239–253
29. Smith, N. V.: Angular Dependent Photoemission. In: Photoemission in Solids I, Topics in Applied Physics, Vol. **26**. Cardona, M., Ley, L. (eds.). Berlin, Heidelberg, New York: Springer 1978, p. 237
30. Feuerbacher, B., Fitton, B., Willis, R. F. (eds.): Photoemission and the Electronic Properties of Surfaces. New York: John Wiley & Sons 1978
31. Rosenblatt, D. H., Kevan, S. D., Tobin, J. G., Davis, R. F., Mason, M. G., Denley, D. R., Shirley, D. A., Huang, Y., Tong, S. Y.: Phys. Rev. **B26**, 1812 (1982)
32. Barton, J. J., Bahr, C. C., Hussain, Z., Robey, S-W., Tobin, J. G., Klebanoff, L. E., Shirley, D. A.: Phys. Rev. Lett., **51**, 272 (1983)
33. Wilch, H.: Atomic and Molecular Scattering from Surfaces — Elastic Scattering. In: Topics in Surface Chemistry. Kay, E., Bagus, P. S. (eds.). New York: Plenum 1978, p. 135
34. Engel, T., Rieder, K. H.: Structural Studies of Surfaces with Atomic and Molecular Beam Diffraction. In: Structural Studies of Surfaces, Springer Tracts in Modern Physics, Vol. **91**. Berlin, Heidelberg, New York: Springer-Verlag 1982, pp. 55–180
35. Savis, F. W., Van der Veen, J. F.: Analysis of Surface Structure and Composition by Ion-Scattering Spectroscopy. In: Proc. 7th Intern. Vac. Congr. & 3rd Intern. Conf. Solid Surfaces, Vienna, 1977, p. 2503
36. Feldman, L. C., Kauffman, R. L., Silverman, P. J., Zuhr, R. A., Barrett, J. H.: Phys. Rev. Lett. **39**, 38 (1978)

37. Heiland, W., Taglauer, E.: Surf. Sci. **68**, 96 (1977)
38. Bell, A. T., Hair, M. L. (eds.): Vibrational Spectroscopies for Adsorbed Species. Washington, D.C.: American Chemical Society 1980
39. Haller, G. T.: Catal. Rev. Sci. Eng. **23**, 477 (1981)
40. Caudano, R., Gilles, J. M., Lucas, A. A. (eds.): Vibrations at Surfaces. New York: Plenum 1982
41. Brundle, C. R., Morawitz, H.: Vibrations at Surfaces. Amsterdam – Oxford – New York: Elsevier 1983
42. Dubois, L. H., Hansma, P. K., Somorjai, G. A.: Appl. Surf. Sci. **6**, 173 (1980)
43. Yates, J. T., Jr., Duncan, T. M., Worley, S. D., Vaughn, R. W.: J. Chem. Phys. **70**, 1219 (1979)
44. Kroeker, R. M., Kasha, W. C., Hansma, P. K.: J. Catal. **61**, 87 (1980)
45. Chiang, S., Tobin, R. G., Richards, P. L.: J. Electron Spectrosc. Relat. Phenom. **29**, 113 (1983)
46. Chang, R. K., Furtak, T. E. (eds.): Surface Enhanced Raman Scattering. New York: Plenum 1981
47. Campion, A.: J. Electron Spectrosc. Relat. Phenom. **29**, 397 (1983)
48. Hall, P. G., Wright, C. J.: Chemical Physics of Solids and Their Surfaces **7**, 89 (1978)
49. Kroeker, R. M., Hansma, P. K.: Catal. Rev.-Sci. Eng. **23**, 553 (1981)
50. Low, M. J. D., Parodi, G. A.: Applied Spectrosc. **34**, 76 (1980)
51. Madey, T. E., Yates, J. T., Jr.: Surf. Sci. **63**, 203 (1977)
52. Knotek, M. L., Jones, V. D., Rehn, V.: Phys. Rev. Lett. **43**, 300 (1979)
53. Winograd, N., Garrison, B. J.: Acc. Chem. Res. **13**, 406 (1980)
54. Madey, T. E., Netzer, F. P., Houston, J. E., Hanson, D. M., Stockbauer, R.: The Determination of Molecular Structure at Surfaces Using Angle Resolved Electron and Photon Stimulated Desorption. In: Proceedings of DIET-I Workshop, Williamsburg, 1982. New York: Springer Verlag (1983)
55. Bradshaw, A. M., Cederbaum, L. S., Domcke, W.: Ultraviolet Photoelectron Spectroscopy of Gases Adsorbed on Metal Surfaces. Structure and Bonding, Vol. **24**. Berlin, Heidelberg, New York: Springer 1975, pp. 133–169
56. Gustafsson, T., Plummer, E. W.: Valence Photoemission from Adsorbates. In: Photoemission and the Electronic Properties of Surfaces. Feuerbacher, B., Fitton, B., Willis, R. F. (eds.). London: Wiley 1978, p. 353–380
57. Rye, R. R., Madey, T. E., Houston, J. E., Holloway, P. H.: J. Chem. Phys. **69**, 1504 (1978)
58. Fuggle, J. C.: High Resolution Auger Spectroscopy of Solids and Surfaces. In: Electron Spectroscopy: Theory, Techniques and Applications, Vol. 4. Brundle, C. R., Baker, A. D. (eds.). New York: Academic Press (1981), pp. 85–152
59. Hagstrum, H. D.: Studies of Adsorbate Electronic Structure Using Ion Neutralization and Photoemission Spectroscopies. In: Electron and Ion Spectroscopies of Solids. Fiermans, L., Vennik, J., Dekeyser, W. (eds.). New York: Plenum 1978, pp. 273–323
60. Johnson, P. D., Delchar, T. A.: Surf. Sci. **77**, 400 (1978)
61. Conrad, H., Ertl, G., Kuppers, J., Wang, S. W., Gerard, K., Haberland, H.: Phys. Rev. Lett. **42**, 1682 (1979)
62. Boiziau, C.: Scanning Electron Microsc. **1982**, 949
73. Citrin, P. H., Eisenberger, P., Hewitt, R. C.: J. Vac. Sci. Technol. **15**, 449 (1978)
64. Stohr, J., Jaeger, R., Brennan, S.: Surf. Sci. **117**, 503 (1982)
65. Stern, E. A., Sayers, D. E., Lytle, F. W.: Phys. Rev. **B11**, 4836 (1975)
66. Stohr, J., Jaeger, R.: Phys. Rev. **B26**, 4111 (1982)
67. den Boer, M. L., Einstein, T. L., Elam, W. T., Park, R. L., Roelofs, L. D.: J. Vac. Sci. Technol. **17**, 59 (1980)
68. Cowley, J. M.: Diffraction Physics. Amsterdam: North Holland 1975
69. Isaacson, M. S., Langmore, J., Parker, N. W., Kopf, D., Utlaut, M.: Ultramicroscopy **1**, 359 (1976)

70. Yagi, K., Takajanagi, K., Kobayashi, K., Osakabe, N., Tanishiro, Y., Honjo, G.: Electron Micrsocopy, 1978, Vol. I (Proc. 9th Intern. Congr. on Ed. Micr., Toronto, 1978). Sturgess, J. M. (ed.). Toronto: Microscopical Society of Canada 1978
71. Yates, J. T., Jr.: The Thermal Desorption of Adsorbed Species. In: Methods of Experimental Physics, Vol. 22, Park, R. L. (ed.). New York: Academic Press (1985), pp. 425–464
72. Holzl, J., Schulte, F. K., Wagner, H.: Work Function of Metals. In: Springer Tracts Mod. Phys. **85**, 1 (1979)
73. Van Hove, M. A., Koestner, R. J., Stair, P. C., Biberian, J. P., Kesmodel, L. L., Bartos, I., Somorjai, G. A.: Surf. Sci. **103**, 189 (1981); **103**, 218 (1981)
74. Adams, D. L., Nielson, H. B., Van Hove, M. A., Ignatiev, A.: Surf. Sci. **104**, 47 (1981)
74a. King, D. A.: Physica Scripta **T4**, 34 (1983)
75. Tong, S. Y., Maldonado, A. L.: Surf. Sci. **78**, 459 (1978)
76. Duke, C. B.: Appl. Surf. Sci. **11/12**, 1 (1982)
77. Chadi, D. J.: Phys. Rev. Lett. **41**, 1062 (1978)
78. Northrup, J. E., Cohen, M. L.: Phys. Rev. Lett. **49**, 1349 (1982)
79. Eastman, D. E.: J. Vac. Sci. Technol. **17**, 492 (1980)
80. Legg, K. O., Jona, F., Jepsen, D. W., Marcus, P. M.: Phys. Rev. **B16**, 5271 (1977)
81. Shih, H. D., Jona, F., Jepsen, D. W., Marcus, P. M.: Phys. Rev. Lett. **46**, 731 (1981)
82. Shih, H. D., Jona, F., Jepsen, D. W., Marcus, P. M.: Surf. Sci. **60**, 445 (1976)
83. Strong, R. L., Firey, B., de Wette, F. W., Erskine, J. L.: J. Electron Spectrosc. Relat. Phenom. **29**, 187 (1983)
84. Behm, R. J., Penka, V., Cattania, M.-G., Kristmann, K., Ertl, G.: J. Chem. Phys. **78**, 7486 (1983)
85. Sachtler, J. W. A., Van Hove, M. A., Biberian, J. P., Somorjai, G. A.: Surf. Sci. **110**, 19 (1981)
86. Somorjai, G. A.: Chemistry in Two Dimensions, Surfaces. Ithaca and London: Cornell University Press (1981)
87. Yates, J. T., Jr., Madey, T. E., Campuzano, J. C. In: The Physics and Chemistry of Solid Surfaces and Heterogeneous Catalysis. King, D. A., Woodruff, D. P. (eds.), in press
88. Kesmodel, L. L., Baetzold, R., Somorjai, G. A.: Surf. Sci. **66**, 299 (1977)
89. Casalone, G., Cattania, M. G., Simonetta, M.: Surf. Sci. **103**, L121 (1981)
90. Casalone, G., Cattania, M. G., Merati, F., Simonetta, M.: Surf. Sci. **120**, 171 (1982)
91. Felter, T., Weinberg, W. H.: Surf. Sci. **103**, 265 (1981)
92. Lloyd, D. R., Quinn, C. M., Richardson, N. V.: Angle-Resolved Ultraviolet Electron Spectroscopy of Clean Surfaces and Surfaces with Adsorbed Layers. In: Surface and Defect Properties of Solids, Vol. VI. Roberts, M. W., Thomas, J. M. (ed.). London: Chemical Society (1976), pp. 179–217
93. Nyberg, G. L., Richardson, N. V.: Surf. Sci. **85**, 335 (1979)
94. Dubois, L. H., Somorjai, G. A.: Surf. Sci. **91**, 514 (1980)
95. Crowell, J. E., Somorjai, G. A.: Appl. Surf. Sci. **19**, 73 (1984)
96. Yang, A. C., Garland, C. W.: J. Phys. Chem. **61**, 1504 (1957)
97. Koestner, R. J., Van Hove, M. A., Somorjai, G. A.: Surf. Sci. **107**, 439 (1981)
98. Van Hove, M. A., Koestner, R. J., Frost, J. C., Somorjai, G. A.: Phys. Rev. Lett. **50**, 903 (1983)
99. Chini, P., Longoni, V., Albano, V. G.: Adv. Organomet. Chem. **14**, 285 (1976)
100. Castner, D. G., Sexton, B. A., Somorjai, G. A.: Surf. Sci. **71**, 519 (1978)
101. Thiel, P. A., Williams, E. D., Yates, J. T., Jr., Weinberg, W. H.: Surf. Sci. **84**, 54 (1979)
102. Koel, B. E., Somorjai, G. A.: J. Electron Spectrosc. Relat. Phenom. **29**, 287 (1983)
103. Lin, R. F., Koestner, R. J., Van Hove, M. A., Somorjai, G. A.: Surf. Sci., **134**, 161 (1983)
104. Van Hove, M. A., Lin, R. F., Koestner, R. J., Koel, B. E., Mate, M., Crowell, J. E., Somorjai, G. A.: LEED and HREELS Studies of Benzene Adsorbed on Rh(111). Proceed. Interdisc. Surf. Sci. Conf. (ISSC-6) April, 1983. University of Warwick, UK, in press
105. Van Hove, M. A., Lin, R. F., Somorjai, G. A.: Phys. Rev. Lett., **51**, 778 (1983)

106. Koel, B. E., Crowell, J. E., Mate, C. M., Somorjai, G. A.: J. Phys. Chem. **88**, 1988 (1984)
107. Lehwald, S., Ibach, H., Demuth, J. E.: Surf. Sci. **78**, 577 (1978)
108. Nieuwenhuys, B. E., Hagen, D. I., Rovida, G., Somorjai, G. A.: Surf. Sci. **59**, 155 (1976)
109. Stair, P. C., Somorjai, G. A.: J. Chem. Phys. **67**, 4361 (1977)
110. Koestner, R. J., Van Hove, M. A., Somorjai, G. A.: J. Phys. Chem. **87**, 203 (1983)
111. Kesmodel, L. L., Dubois, L. H., Somorjai, G. A.: J. Chem. Phys. **70**, 2180 (1979)
112. Koestner, R. J., Van Hove, M. A., Somorjai, G. A.: Surf. Sci. **121**, 321 (1982)
113. Skinner, P., Howard, M. W., Oxton, I. A., Kettle, S. F. A., Powell, D. B., Sheppard, N.: J. Chem. Soc., Faraday Trans. 2, **77**, 1203 (1981)
114. Dubois, L. H., Castner, D. G., Somorjai, G. A.: J. Chem. Phys. **72**, 5234 (1980)
115. Koel, B. E., Crowell, J. E., Bent, B. E., Mate, C. M., Somorjai, G. A.: J. Phys. Chem., to be published
116. Ibach, H., Mills, D. L.: Electron Energy Loss Spectroscopy and Surface Vibrations. New York: Academic Press (1982), p. 326
117. Gates, J. A., Kesmodel, L. L.: Surf. Sci. **124**, 68 (1983)
118. Minot, C., Van Hove, M. A., Somorjai, G. A.: Surf. Sci. **127**, 441 (1982)
119. Avery, N., et al.: to be published and private communication